OPTICAL CHARACTERIZATION OF ANTIMONY-BASED, TYPES-I AND -II, MULTIPLE QUANTUM-WELL SEMICONDUCTOR STRUCTURES FOR MID-INFRARED LASER APPLICATIONS

THESIS

Edward G Ferguson, 2Lt, USAF

AFIT/GAP/ENP/03-04

DEPARTMENT OF THE AIR FORCE
AIR UNIVERSITY

AIR FORCE INSTITUTE OF TECHNOLOGY

Wright-Patterson Air Force Base, Ohio

AFIT/GAP/ENP/03-04

OPTICAL CHARACTERIZATION OF ANTIMONY-BASED, TYPES-I AND -II,

MULTIPLE QUANTUM-WELL SEMICONDUCTOR STRUCTURES FOR MID-

INFRARED LASER APPLICATIONS

THESIS

Presented to the Faculty

Department of Engineering Physics

Graduate School of Engineering and Management

Air Force Institute of Technology

Air University

Air Education and Training Command

In Partial Fulfillment of the Requirements for the

Degree of Master of Science (Applied Physics)
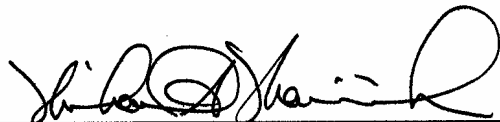
Edward G Ferguson, BS

2nd Lieutenant, USAF

March 2003

OPTICAL CHARACTERIZATION OF ANTIMONY-BASED, TYPES-I AND -II,

MULTIPLE QUANTUM-WELL SEMICONDUCTOR STRUCTURES FOR MID-

INFRARED LASER APPLICATIONS
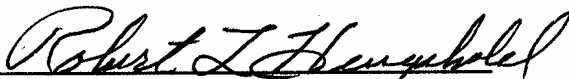
Edward G Ferguson, BS
2Lt, USAF

Approved:

Lt. Col. Michael A. Marciniak, Advisor	11 Mar 03
	date
Dr. Robert L. Hengehold, Member	11 Mar '03
	date
Dr. David E. Weeks, Member	11 Mar 03
	date

Preface

      Getting this degree has been a challenging and rewarding experience. The classes I took and the people I met along the way will stay with me forever. The AFIT staff was always behind me and in some cases out pulling me. Greg and Mike were always there to get my lab equipment working again and always willing to give their time and help whenever I needed it. When I was looking for a direction LTC Marciniak always guided me where I needed to go. I could never have gotten the modeling portion of this thesis started if it weren't for Dr. Weeks. The staff at AFIT was only the tip of the help I got along this journey.

      My family and girlfriend were always willing to lend an ear or let me bounce an idea off of them. Ron helped me get out and learn things besides academics. There are few things as important to me as the friends I had, and the friends I made here at AFIT. I could never have finished this without you all.

                                           Edward G. Ferguson

Table of Contents

List of Figures

List of Tables

Abstract

This experiment characterizes antimony-based, multiple quantum-well, types-I and -II, semiconductor samples designed for laser applications. The samples emit light in the 3-5-μm range to exploit an atmospheric transmission window, making them ideal for infrared (IR)-seeking missiles countermeasures. Photoluminescence (PL) spectra were collected and yielded bandgap (E_g) dependence-on-temperature relationships. The type-I sample was found to follow the Varshni equation, while the type-II samples showed a rise with temperature in a portion of the curve that should be linear according to the Varshni equation. The type-II samples followed the Varshni equation well at higher temperature. The PL study indicated that the type-I sample had better efficiency than the type-II samples, and that there is some change in efficiency with the waveguide nature of the sample. Carrier temperatures (T_c) were derived from the PL study, all the samples for which T_c was derived operated in the optical phonon regime. The PL data was compared to the "FEMB" computer model and some correlation between the two in recombination energy was seen. A time resolved photoluminescence (TRPL) experiment was conducted using the frequency upconversion technique. The experiment clearly found the upconverted signal, but there was a systematic error that prevented any further analysis of the data.

OPTICAL CHARACTERIZATION OF ANTIMONY-BASED, TYPES-I AND -II,

MULTIPLE QUANTUM-WELL SEMICONDUCTOR STRUCTURES FOR MID-

INFRARED LASER APPLICATIONS

1. Introduction

Semiconductor lasers have applications in communications, spectroscopy, environmental detection, biomechanical devices, and infrared (IR) countermeasure devices. The small size, reliability of lasing and ease of use make these lasers ideal for military uses. The intensity of emitted radiation currently limits the uses of semiconductor laser devices. The purpose of this experiment is to characterize a set of semiconductor materials. Sample characteristics are determined by optically exciting a sample, which causes it to emit radiation, and collecting the intensity of the luminescence as a function wavelength (photoluminescence). By varying the excitation power or sample temperature, different characteristics of a semiconductor material are determined. The photoluminescence (PL) results are compared to results provided by the **femb** computer code. PL provides time-averaged characteristics; by using a wave mixing technique (upconversion), temporal characteristics can be determined (time-resolved photoluminescence).

The samples in this experiment are antimony-based (Sb) structures. The atmosphere has transmission windows in the 3-5-μm region, which are exploited by

1

current IR missile technology. An optical countermeasure to these devices should

propagate at similar wavelengths. Figure 1.1 below shows the correlation between III-V

semiconductor material composition and transmission windows in the atmosphere. The

solid lines connecting the binary compositions indicate where a ternary compound would

emit at the wavelength indicated along the upper x-axis or at the energy specified on the

lower x-axis. Following the gray line up to the chart of transmission windows, the

window exploited by a certain material composition is indicated. Antimony-based

structures exploit the necessary atmospheric transmission windows to counter IR

missiles, as indicated in Figure 1.1, specifically the 3.5 to 4.2 μm and 4.4 to 5.4 μm

transmission windows.
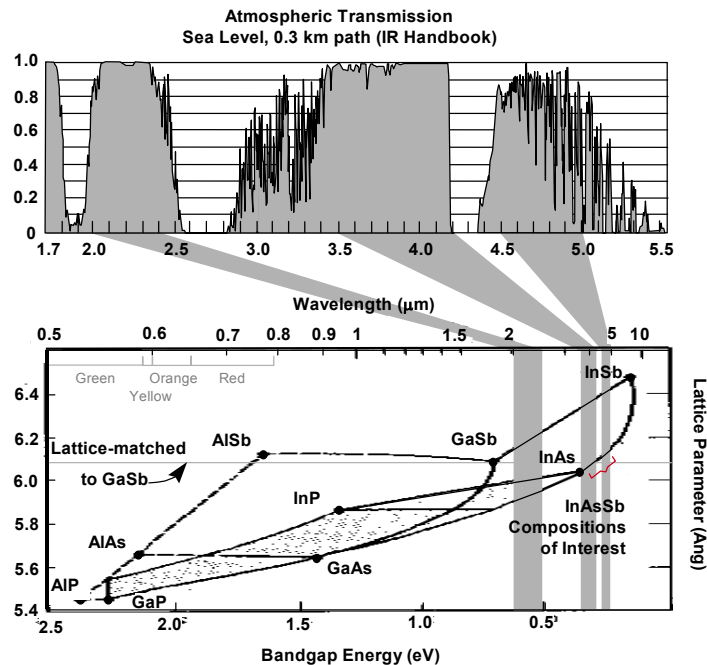
Figure 1.1. Atmospheric transmission windows and the material compositions that emit
in those wavelengths (Marciniak, 1995:1-3)

1.1 Motivation

In Operation Dessert Storm, 80% of fixed wing aircraft losses were due to IR missiles (Pike, 2000). Since the Gulf War, 80-90% of aircraft losses have been due to IR missiles (Rockwell, 2002). An IR missile launched one mile away gives a pilot approximately four seconds to deploy countermeasures; this is not enough time for a human to react and get away. Due to the current IR missile threat, the Air Force is generally flying its aircraft above 15,000 ft., which is outside the range of IR guided surface-to-air missiles (SAM's) (Erwin, 2002). These altitudes reduce the munitions accuracy and diminish ground reconnaissance and target detection capabilities (Rockwell, 2002).

The large proliferation of both vehicle launched and man-portable (MANPAD) IR missiles has increased the need for IR missile counter measures. Bill Taylor, of the Air Force Research Laboratory's Electro-Optical Technology Division, has said that by 2005 IR missiles can be expected to defeat flares nearly 100% of the time (Green, 1999). The growing threat and the increasing ability of IR missiles to defeat countermeasures require a new defense to be created.

Presently, a Large Aircraft Infrared Countermeasures (LAIRCM) system is being developed by the Air Force. The requirement of the system is to protect against man-portable, shoulder-fired, and vehicle-launched IR-guided missiles. "The LAIRCM system will be installed on C-17, C-130 and KC-135 aircraft. There are five basic elements to this system: a Control Indicator Unit (CIU), a Missile Warning Subsystem (MWS), a Pointer/Tracker Transmitter (P/T), a Countermeasures Processor (CP), and a Laser jam source subsystem. Up to three laser jammers will be installed on every aircraft

(Christie, 2002)." With the development of semiconductor lasers, the size and power requirements of the three laser components could be dramatically reduced, making it possible to place similar units on fighter aircraft, as well as reducing the cost of the system. The development of semiconductor lasers makes it possible for lives to be saved and the mission to be executed.

1.2 Overview

This experiment characterizes a set of type-I and type-II multiple-quantum-well (MQW), Sb-based structures. It compares a tight and diffuse waveguide type-II MQW structure with a photoluminescence (PL) study. Finally, a time-resolved photoluminescence (TRPL) study is attempted. The PL study yields bandgap-energy (E_g) dependence on temperature (T), carrier temperatures (T_c), and each samples optical-to-optical efficiency. The results of the PL study prompted a modeling effort to determine if a commercially available **femb** code would predict the observed results. A TRPL experiment yielded results that clearly showed the experiment was functioning, but the signal-to-noise ratio of the results was not high enough to further analyze the data. An alignment problem is believed to have caused this. Future work is suggested after the results of this experiment have been presented and analyzed.

2. Background

This chapter will explain the basic characteristics of energy bands, types of carrier recombination, and type-I and type-II semiconductor quantum-well (QW) structures. It will also discuss previous work performed in similar areas of research. Energy bands are determined by the structure of the material, and they in turn determine the energy absorbed and emitted by the material. Recombination occurs when an excited electron loses its excess energy and fills a vacant state in a lower (valance) energy band. Radiative recombination is one of three possible types of recombination; Shockley-Read-Hall and Auger are the other two. Type-I and type-II semiconductors are different QW structures used to enhance carrier confinement and optimize radiative recombination. The most fundamental of all of semiconductor characteristics is the energy band.

2.1 Energy Bands

The atoms present in a semiconductor determine energy bands. A band is formed as atoms are moved closer to one another. The highest discreet energy levels in a single atom merge to form a range of allowable energy states, identified as bands. Figure 2.1 illustrates this process for silicon. The 2P and 2S energy levels in an individual atom combine with the same energy levels in other atoms and broaden. At a separation of 11 lattice constants, the formation of bands begins to appear. The lattice constant is the equilibrium interatomic spacing of the crystal lattice (McKelvey, 1993: 63).
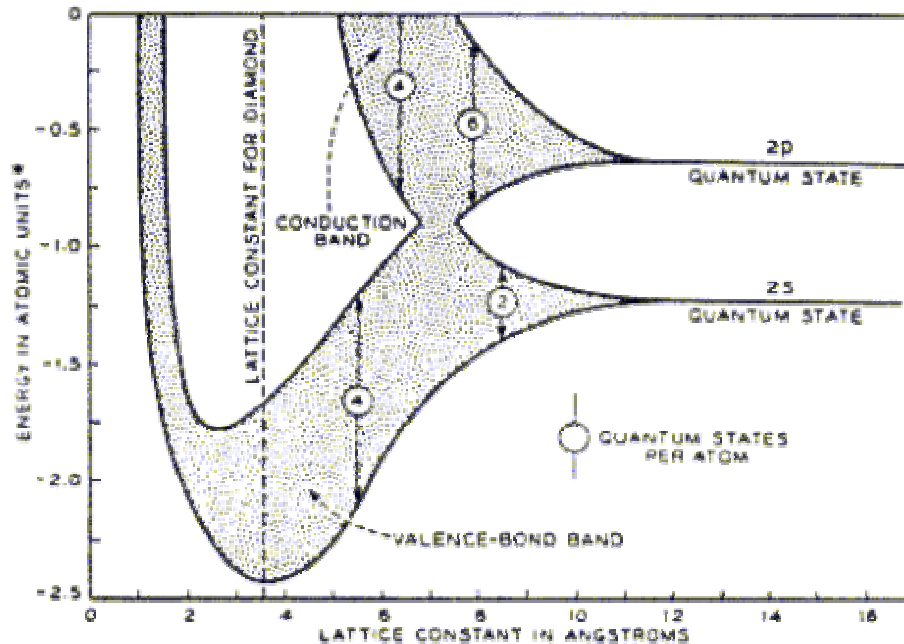
Figure 2.1. As atoms in a lattice are pushed closer together the energy levels in the individual atoms begin to form energy bands (Zeghbroeck, 2002).

The formation of the crystal lattice structure is dependent on the type and strength of bonds formed between atoms. The lattice structure determines the bandgap energy, conduction band energy, valence band energy and any impurity band energies. Typical diagrams, such as Figure 2.2, are used to illustrate band energies.

In a semiconductor, the energy levels of the conduction and valence bands are determined at temperature (T) equal to 0 K. The bottom of the conduction band is defined as the lowest unfilled energy level at T= 0 K; the top of the valence band is the highest filled energy level at T = 0 K. The difference between these two energy levels is the bandgap energy (E_g). E_g determines the wavelength of absorbed light because an incoming photon with energy lower than the bandgap travels through the material, where

6

as an incoming photon at a higher energy is absorbed, losing its energy by generating free

carriers in the material.
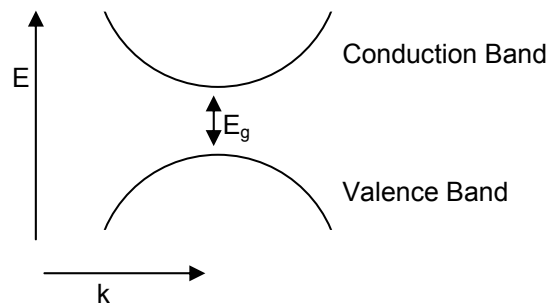
Figure 2.2. Typical energy diagram; E_g= bandgap energy

2.2 Free Carriers

When an electron is excited into the conduction band, there is an unfilled state left

in the valance band. The number of electrons in the valance band is on the order of 10^{23};

because of the large number of electrons in the valance band, it is simpler to count the

number of vacancies in the band. These vacancies are given the name "holes." Free

carriers are holes in the valance band and electrons in the conduction band.

2.3 Recombination

All things in nature tend towards lowest energy; therefore, in a given amount of

time, the excited electrons in a crystal lattice will "fall" to lowest energy. When an

electron from a higher band fills a hole in a lower band, its energy must be given off.

The process of an electron filling a hole and giving off energy is called recombination.

The type of recombination is dependent on the way in which the electron gives off its

energy.

2.3.1 Shockley-Read-Hall Recombination

Shockley-Read-Hall recombination occurs when an electron gives its energy to

the crystal lattice in the form of a phonon. This process occurs when an electron relaxes

to an intermediate energy level caused by an impurity and then relaxes to its lowest

energy in the valence band. This process involves one carrier; it is illustrated in Figure

2.3.
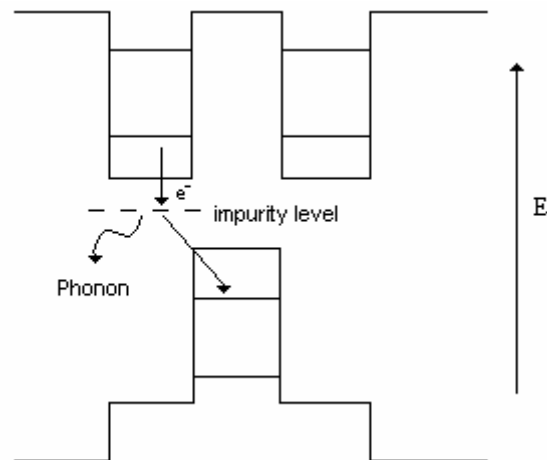
Figure 2.3. In Shockley-Read-Hall recombination, electrons lose their energy, in the form
of phonons to the crystal lattice with the assistance of an impurity energy level.

2.3.2 Radiative Recombination

Radiative recombination occurs when a carrier loses its energy to a photon. The electron combines directly with a hole in the valence band in a single step two carrier (electron and hole) process. The energy given off is usually the same as the material E_g. This process is shown in Figure 2.4.
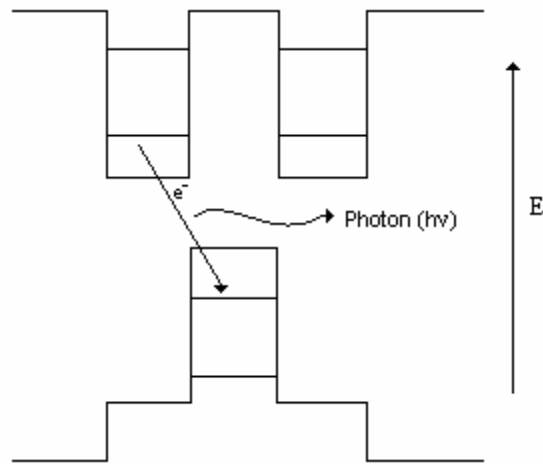
Figure 2.4: In radiative recombination, an electron losses its energy in the form of a photon with energy $\Delta E = h\nu$.

2.3.3 Auger Recombination

Auger recombination occurs when an electron in the conduction band recombines with a hole in the heavy-hole (HH) valance band but instead of losing its energy to a photon, it gives its energy to an electron in the split-off (SO) valance band, which is promoted to a hole state in the HH band. This is type of Auger recombination is called

conduction, heavy-hole, heavy-hole, split-off (CHHS) Auger recombination and is a two-

step, three-carrier process. The probability of CHHS Auger recombination is based on

how close the difference between the SO and HH bands is to the bandgap energy. Figure

2-7 describes this process. The probability of Auger recombination is related to the

energy difference (ΔE) between the SO and HH-bands and its relation to E_g. If the

difference between the SO band and HH band energies are close to E_g, then the

probability of Auger recombination goes up.
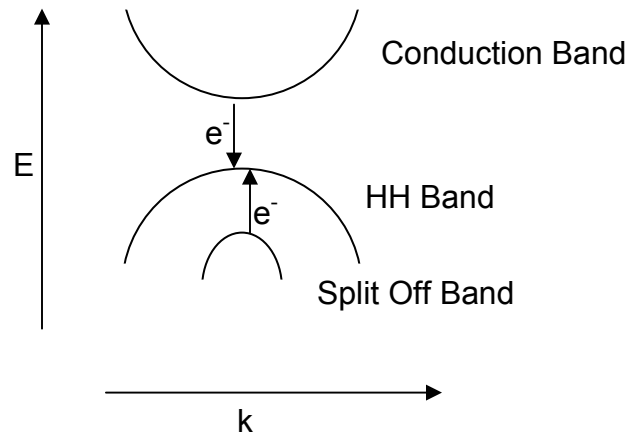
Figure 2.5. In Auger recombination an electron in the conduction band recombines with a
hole in the heavy-hole (HH) valance band but instead of losing it's energy to a photon, it
gives its energy to an electron in the split-off (SO) valance band, which is promoted to a
hole state in the HH band.

2.4 Material Structures

Semiconductor materials can be grown into several different structure types. By alternating the thickness and type of a layer, quantum well structures can be grown into a semiconductor material. Quantum wells are formed when a high-bandgap material is grown next to a low bandgap material, and then a second layer of high-bandgap material finishes the well. The quantum wells grown into a sample have similar properties to the single quantum well or "particle in a box" solutions. The transitions seen in quantum-well semiconductors should be between the lowest allowed energy levels in the quantum wells. Quantum well structures increase carrier confinement because they are grown such that the lowest allowed quantum-well energy level is lower than the lowest energy level of the material on either side of the well, this forces free carriers to collect in the bottom of the well. This process increases carrier confinement and that, in turn, increases radiative transitions in a semiconductor. When multiple quantum-well layers are grown into a material, it is a multiple-quantum-well structure (MQW). Type-I structures have the quantum wells for the electrons and the quantum wells for the holes in the same material, or lined up over one another spatially, as shown in Figure 2.6.
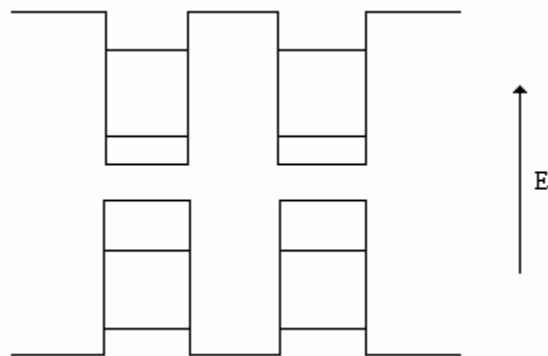
Figure 2.6. Type-I MQW structure

Type-II MQW structures have the quantum wells for the electrons and the quantum wells for the holes in adjacent materials, which creates spatially offset quantum wells as shown in Figure 2.7
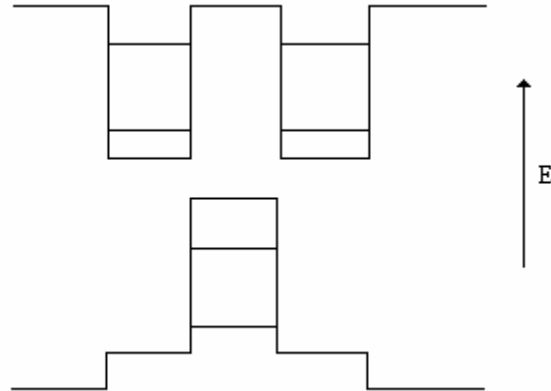
Figure 2.7. Type-II MQW structure

2.5 Previous Work

Previous Air Force Institute of Technology (AFIT) students, McKay and Gorski, described some of the samples in the photoluminescence (PL) study in work in their Master's theses. In those documents, the upconversion technique, described later in Chapter 3, was used to determine recombination coefficients, time-dependent carrier temperatures, and other material characterization parameters. In addition to characterization with the upconversion technique, simple PL data is presented and was obtained to identify the peak emission wavelength of the samples. This experiment uses the same techniques described in McKay's and Gorski's theses (McKay, 2000 and Gorski, 2002). Batacharia describes many of the techniques that can be used to obtain PL

data and what some of the characteristics that can be seen in the data are. Marciniak presents PL data and techniques in his dissertation (Marciniak, 1995). His dissertation also contains analysis similar to that given in this experiment for bulk materials. All of these documents were used heavily in the formulation of experiments performed and in the analysis of the data taken.

3. Experiment

Photoluminescence (PL) is the result of electron and hole recombination. The excited electron gives off energy as it decays to a lower energy state according to Equation (Eq) (3.1).

$$\lambda = \frac{hc}{\Delta E} \qquad (3.1)$$

The wavelength, λ, of the emitted light is directly proportional to Planck's constant, h, and the speed of light in a vacuum, c, and inversely proportional to the energy, ΔE, given up by the electron when it combines with a hole. A PL study requires, at a minimum, a way to excite the sample and a way to collect and measure the light emitted by the sample as a result of excitation. A time-resolved photoluminescence (TRPL) study requires a non-linear crystal as well as the previously mentioned components. This chapter describes the samples characterized, the equipment used for both PL and the TRPL experiments, the layout of that equipment, and the theory behind the techniques used.

3.1 Samples

The samples in this experiment are a combination of type-I and type-II QW Sb-based semiconductor materials. In addition to the differences in QW structure, diffuse

and strong waveguide structures are examined. The compositions of the sample materials

are given Table 3.1. Figure 3.1 is a diagram of the active regions of the samples.

Table 3.1. Compositions of the sample set.

Sample	Composition	Absorber	Structure	Cladding
B	$InAs_{0.935}Sb_{0.065}/In_{0.85}Al_{0.15}As_{0.0.9}Sb_{0.1}$		Type-I	none
R0-62	$InAs/Ga_{0.65}In_{0.35}Sb$	$In_{0.15}Ga_{0.85}As_{0.08}Sb_{0.92}$	Type-II	$Al_{0.90}Ga_{0.10}As_{0.08}Sb_{0.92}$
R2-43	$InAs/Ga_{0.65}In_{0.35}Sb$	$In_{0.15}Ga_{0.85}As_{0.08}Sb_{0.92}$	Type-II	none
G	$Ga_{0.15}In_{0.08}Sb/InAs/Ga_{0.85}In_{0.15}Sb/InAs$	$In_{0.15}Ga_{0.85}As_{0.08}Sb_{0.92}$	Type-II	none
R1-73	$InAs/Ga_{0.60}In_{0.40}Sb$		Type-II	none
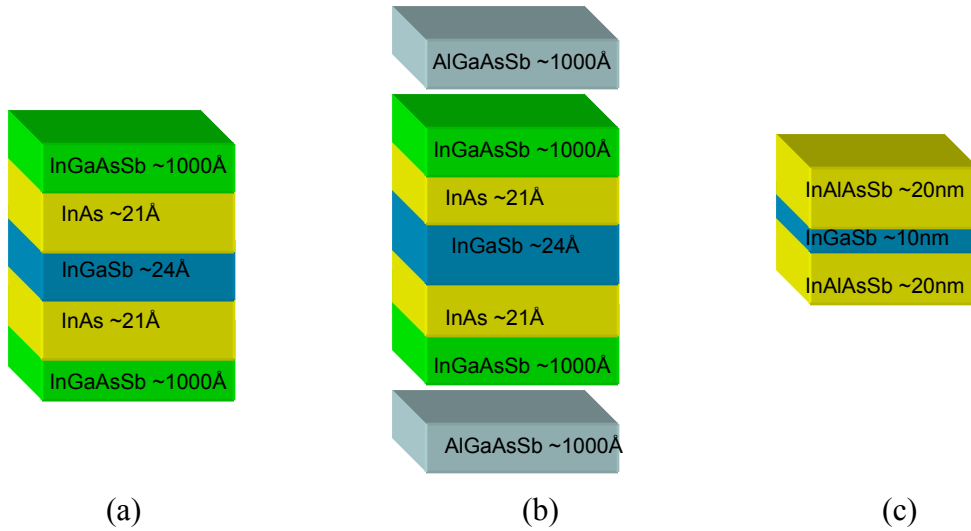
Figure 3.1. Diagrams of the active regions for each of the samples. (a) is for samples R0-62, G, R1-73. (b) is a diagram of sample R2-43's active region and shows were the cladding layer is with respect to the active region. (c) is a diagram of sample B

A tight waveguide has a low index of refraction cladding layer grown on both sides of the higher index of refraction active region. The active region of a material is the location of the recombination. For these samples the active region is composed of the quantum well structures.

3.2 Layout

Figure 3.1 shows the table layout for the experiment. An argon-ion (Ar$^+$) laser is used to pump a mode locked Ti:sapphire laser that is used to excite the sample. The PL path, shown by a solid line, passes through an empty crystal mount/rotation stage and is collected by a ½-m spectrometer. The sum frequency generation (SFG) signal, shown by a long dashed line, is generated in a nonlinear KTiOAsO$_4$ (KTA) crystal and collected in a ¾-m spectrometer.

3.3 Photoluminescence

The vertically polarized beam, which shall be called the PL beam, exits the beam splitter and is directed through a neutral density filter and onto to a 30-cm delay stage. The delay stage is a gold-coated retro-reflector on a sliding mount that is controlled by the upconversion computer program. The sliding mount becomes important to the upconversion experiment and will be discussed in detail in Section 3.3. The PL beam is then focused onto the sample mounted in the cryostat with a spot size of 58.5 +/- 0.20 μm (Gorski, 2001:22).
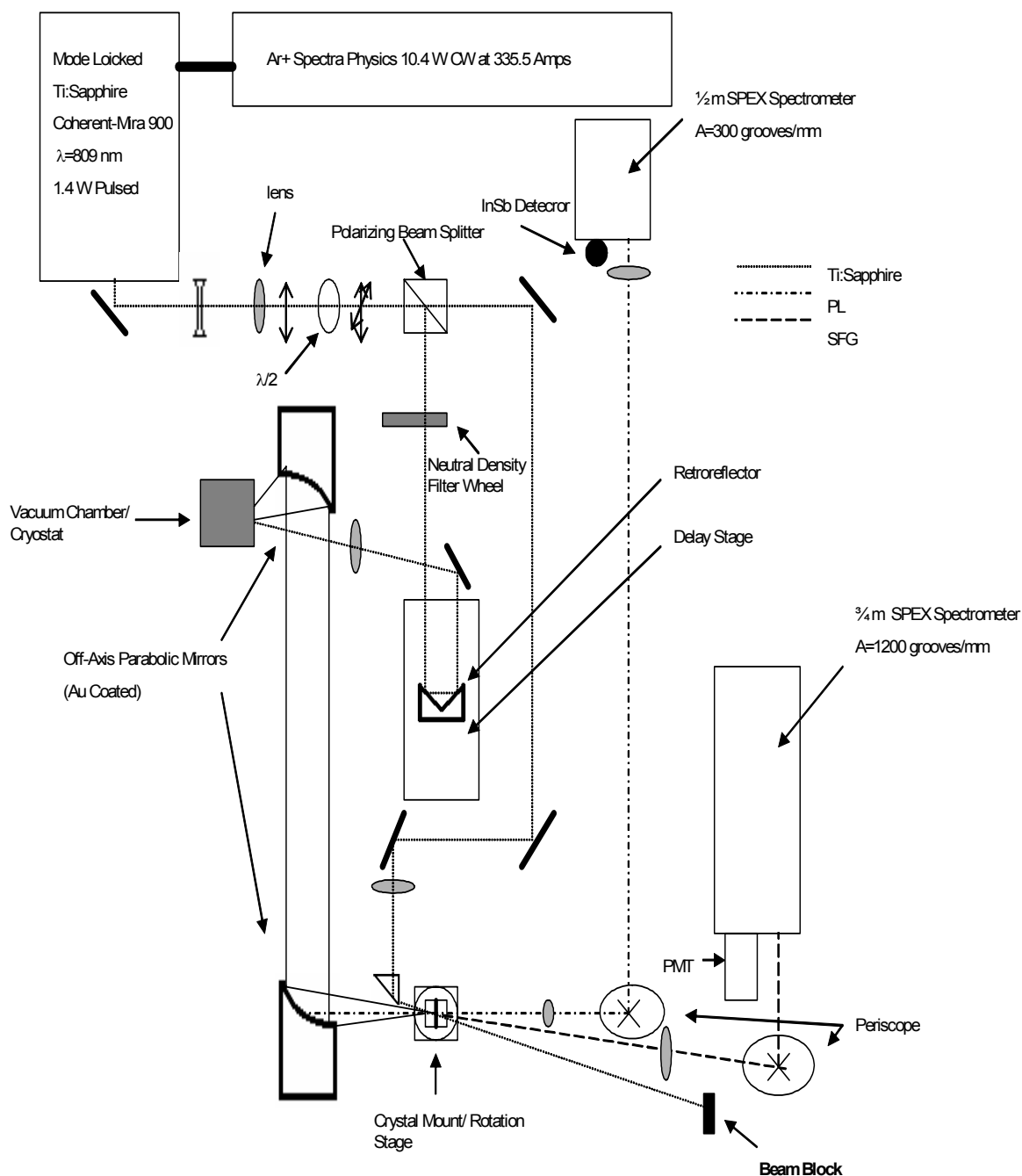
Figure 3.2. A Ti:sapphire beam is used as the sample excitation source. It is split into two paths at a polarizing beam splitter. The vertically polarized PL beam then travels through a delay stage before exciting a sample. The luminesence is then sent to a periscope and on into a ½ m spectrometer for PL, or into the KTiOAsO$_4$ (KTA) crystal for upconversion. After the beam splitter the horizontally polarized Ti:sapphire is mixed with the PL in the KTA to generate a sum-frequency generated (SFG) signal which is then directed into a ¾ m spectrometer and photon counter.

The gold-coated off-axis parabolic mirror then collects the luminescence from the sample and collimates it. The luminescence is directed toward a second gold-coated off-axis parabolic mirror and focused onto a crystal mount/rotation stage. When performing the PL experiment, there is no crystal in the crystal mount/rotation stage. A CaF$_2$ lens collects the luminescence of the sample and collimates it so that it can be vertically raised by a periscope and focused by a second CaF$_2$ lens onto the entrance slits of a ½-m SPEX spectrometer. At the exit slit of the ½-m spectrometer, the luminescence is focused by a CaF$_2$ lens onto a single element indium antimonide (InSb) detector to detect incident photons. The InSb detector will detect emissions in the 2- 5.56-μm range.

Eq (3.2) determines the resolution of the ½-m spectrometer.

$$\Delta\lambda = \frac{aW}{mf} \qquad (3.2)$$

Resolution, $\Delta\lambda$, of a spectrometer is directly proportional to the grooves per mm of the grating, a, the slit width, W, and is inversely proportional to the order of the diffraction observed, m, and the focal length of the spectrometer, f. Both the spectrometer resolution and the wavelength step size between subsequent data points determine the resolution of the experiment. The larger of the two is the resolution of the experiment, and is 5 nm or 6 nm for the experiment depending on the sample in question. The PL beam is chopped at 200 MHz so that a Stanford Research Systems SR 850 DSP lock-in amplifier can amplify the signals from InSb detector.

The PL experiment yields data in the form of intensity as a function of wavelength. By varying the excitation power incident upon the sample or the sample

temperature, one can characterize carrier temperature, E_g, and the sample's optical-to-optical efficiency.

3.4 The Upconversion Technique

The time evolution of the PL signal can be determined using Time-Resolved Photoluminescence (TRPL). There are several techniques, streak cameras and frequency upconversion being among the most used, that can be used to get TRPL data. Each technique is used to investigate both carrier relaxation and carrier transport. Using fast detectors and fast electronics gives these properties directly. Streak cameras can provide sub-picosecond resolution in a single-shot operation and ~10 ps resolution in synchroscan mode for low-level repetitive signals (Shah, 1999). This experiment uses the frequency upconversion technique because streak cameras are not available detect mid-IR signals. Even if they were, the resolution of the frequency upconversion technique is much higher than that of a streak camera. The excitation laser pulse is the ultimate limit to the resolution of the frequency upconversion technique.

As mentioned in Section 3.3, the ultrafast excitation laser beam is separated into two portions by the polarizing beam splitter. The first portion of the excitation beam stimulates a sample and produces PL, which is focused onto a nonlinear crystal, KTA. The horizontally polarized portion of the excitation beam (pump beam) travels a similar path length and is also focused into the nonlinear crystal for mixing with the PL signal. Varying the path length of the beams relative to one another allows the nonlinear mixing to occur with various temporal portions of the PL signal, thereby yielding the time

development of the PL signal (Figure 3.2). This information provides for the

characterization of recombination and carrier transport.
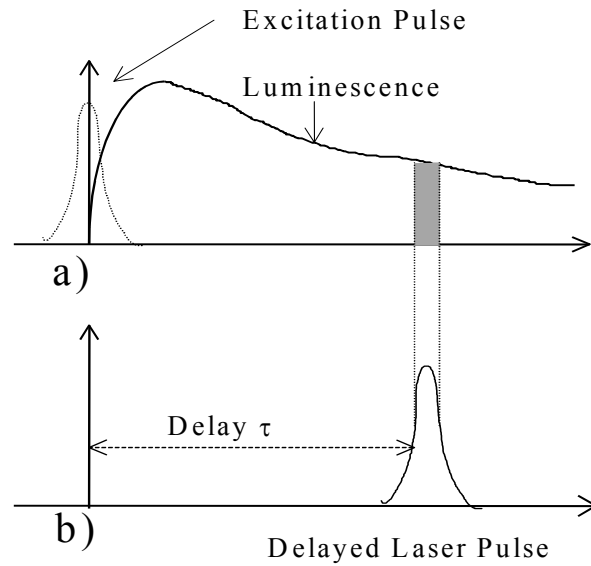
Figure 3.3. The PL and excitation laser pulses mix to form a third sum-frequency generated (SFG) signal. (a) shows the PL signal in time. (b) depicts the way varying the path length of the PL and excitation pulses relative to one another allow the PL beam to be examined at different times.

The sample is stimulated in the same manner as the PL experiment. The

frequency upconversion occurs at the crystal mount/ rotation stage. The mount now

holds a KTA crystal exhibiting second-order nonlinearity. Further information on the

crystal can be found in Gorski's thesis (Gorski, 2002). After the PL beam is focused on

the KTA, the beam is blocked so it is not collected in the ¾-m spectrometer used to

collect the SFG signal. The pump beam traverses a similar distance to the PL beam and is then focused through a lens to a spot size of 39.1 +/- 0.15 μm (Gorski, 2001:22) onto the KTA crystal, and then blocked after the crystal to prevent it from being collected in the ¾-m spectrometer. There are also filters for the laser wavelength in the SFG signal path to the spectrometer and over the entrance slit to the spectrometer to further reduce any chance of collecting the laser beam in the ¾-m spectrometer. The SFG signal is collimated by a lens and then raised to the level of the spectrometer by a periscope. The signal enters the spectrometer and is measured with a photo multiplier tube (PMT).

The SFG signal is only produced if the PL and pump beams overlap in space. To accomplish this alignment, a 50-μm pinhole is placed in the crystal mount/ rotation stage and both beams are directed through it to ensure this overlap. In order to find the temporal beginning of the PL signal, a process to find zero-path-length (ZPL) difference between the two beam paths from the beam splitter to the cryostat/ rotation stage is performed. At ZPL, the pump pulse is aligned in time with the beginning of the PL signal. This point is found after the beams are overlapped in space by exchanging the 50-μm pinhole for a LIO_3 crystal. A visual check for this point is a purple point of light generated by mixing the pump beam with the PL excitation laser beam reflected off the sample mount and directed along the PL path to the LIO_3 crystal.

There are two conditions to generate this signal, the first of which is phase matching, mathematically defined by Eq (3.3).

$$\vec{k}_{up} = \vec{k}_{PL} + \vec{k}_{pump} \qquad\qquad (3.3)$$

$\vec{k}_{up}$ is the propagation vector of the ZPL or SFG signal and is the vector sum of the PL

beam propagation vector, $\vec{k}_{PL}$, and the pump beam propagation vector $\vec{k}_{pump}$. By solving

Eq (3.3), one can also obtain the angles at which the PL and pump beams must intersect

each other in the KTA crystal and the angle at which the KTA should be cut. The

derivations of this information and more detail about the upconversion experiment can be

found in Gorski's thesis (Gorski, 2002). The angle of the crystal face relative to normal

to the X-Z plane used here is 43°, and the beams should intersect in the crystal at an angle

of 20° from the normal to the X-Z plane (Gorski, 2002).

The second condition for ZPL or SFG signal generation is a frequency matching

condition given in Eq (3.4), where ω_{up} is the frequency of the SFG signal, ω_{PL} is the

frequency of the PL pulse, and ω_{pump} is the frequency of the pump beam. By

manipulating Eq (3.4) using the relationship between frequency and wavelength, Eq

(3.5), one can obtain the wavelength of the ZPL signal using Eq (3.6).

$$\omega_{up} = \omega_{PL} + \omega_{pump} \qquad (3.4)$$

$$c = \frac{\omega\lambda}{2\pi} \qquad (3.5)$$

$$\frac{1}{\lambda_{up}} = \frac{1}{\lambda_{PL}} + \frac{1}{\lambda_{pump}} \qquad (3.6)$$

The wavelength of the SFG or ZPL signal, λ_{up}, is dependent upon the wavelength of both the PL signal and the pump beam, represented by λ_{PL} and λ_{pump}, respectively. The upconversion technique produces a curve of the intensity as a function of the delay time between the PL and pump beams.

3.5 Excitation Source

Both PL and upconversion require a way to excite the sample. A 10.2 W continuous wave (CW) Spectra Physics argon-ion (Ar^+) laser pumped the mode-locked Ti:sapphire. In upconversion, the pulse width of the excitation source determines the temporal resolution of the experiment. The excitation source for this experiment was a Coherent Mira 900 mode-locked Ti:sapphire laser. It operated at 1.4 W average power and produced ~120 fs pulses that were used to excite the sample. The laser has an average wavelength of 810 nm and has a repletion rate of 76 MHz. The sample is excited every 13.2 ns by mode-locked pulses. In the photoluminescence study, the laser is chopped at 200 MHz in order to provide a signal for the lock-in amplifier. The pulse width used in the upconversion experiment is measured using an INRAD Model 5-14BX Autocorrelator and checked using the experiment equipment. The ZPL signal is the point where the two portions of the initial excitation pulse are recombined in the nonlinear crystal. By changing the delay between the pulses, a representation of how the excitation pulse develops in time is generated just as the representation of the development of the PL signal. The autocorrelator does this in a "black box" unit and the delay stage in the PL beam path combined with the ¾ m spectrometer, tuned to the ZPL wavelength, performs this experiment in the exact same way. The pulse width of the Ti:sapphire laser

was measured to be 125 fs. The output value of the both of the lasers was constant from

day to day which allowed the experiment to be run at greater time efficiency.

4. Data and Analysis

This chapter will present the data collected for each sample. The data was collected versus temperature or excitation power. Effective carrier temperatures will be extracted from intensity versus wavelength data as a function of excitation power data. In addition, gain saturation will be examined, as will E_g variances with temperature and excitation power. PL observations will then be compared to a commercially available **femb** computer model for semiconductor structures. Finally, the results of a TRPL study will be presented.

4.1 Photoluminescence

Taking the PL data at the same excitation power and varying the sample temperature can determine the effects of temperature on a material. The most noticeable effect of temperature is usually a change in E_g. Figure 4.1 shows the PL data as a function of temperature for sample G and is indicative of the data for the experiment sample set. Figure 4.2 shows the PL data for sample R0-62. An E_g change is indicated by a change in the position of the peak intensity. Both Figure 4.1 and Figure 4.2 clearly show the change in E_g with temperature. The reduction in signal in Figure 4.2 between ~2.85 eV and ~2.95 eV is the result of atmospheric, primarily CO_2, absorption. The energies/ wavelengths affected by this absorption can be seen in Figure 4.3.
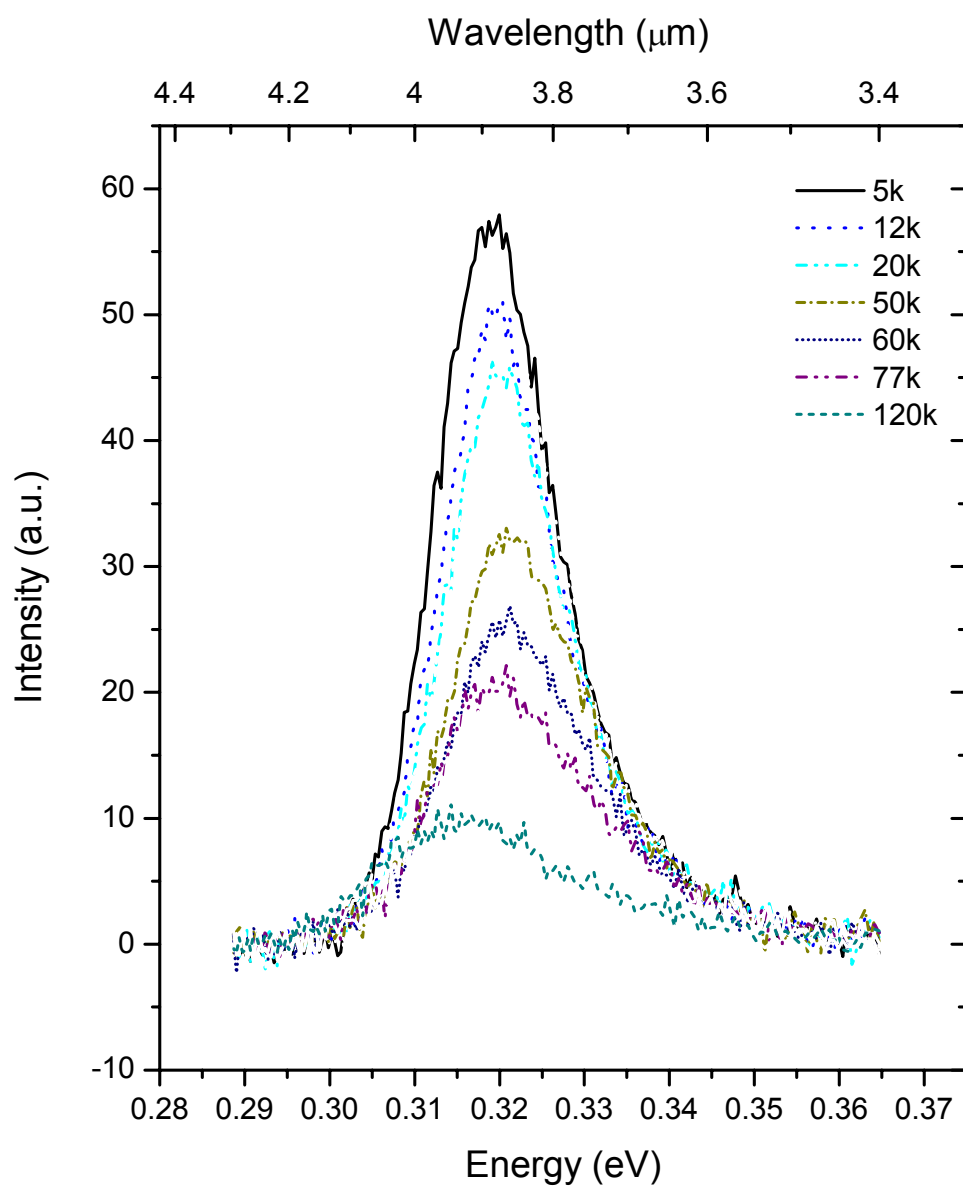
Figure 4.1. Sample G intensity as a function of energy at varying temperatures. The resolution in temperature is 4K. The wavelength resolution is 5nm and the energy resolution is 8.6meV. This plot clearly shows that E_g varies as a function of temperature.
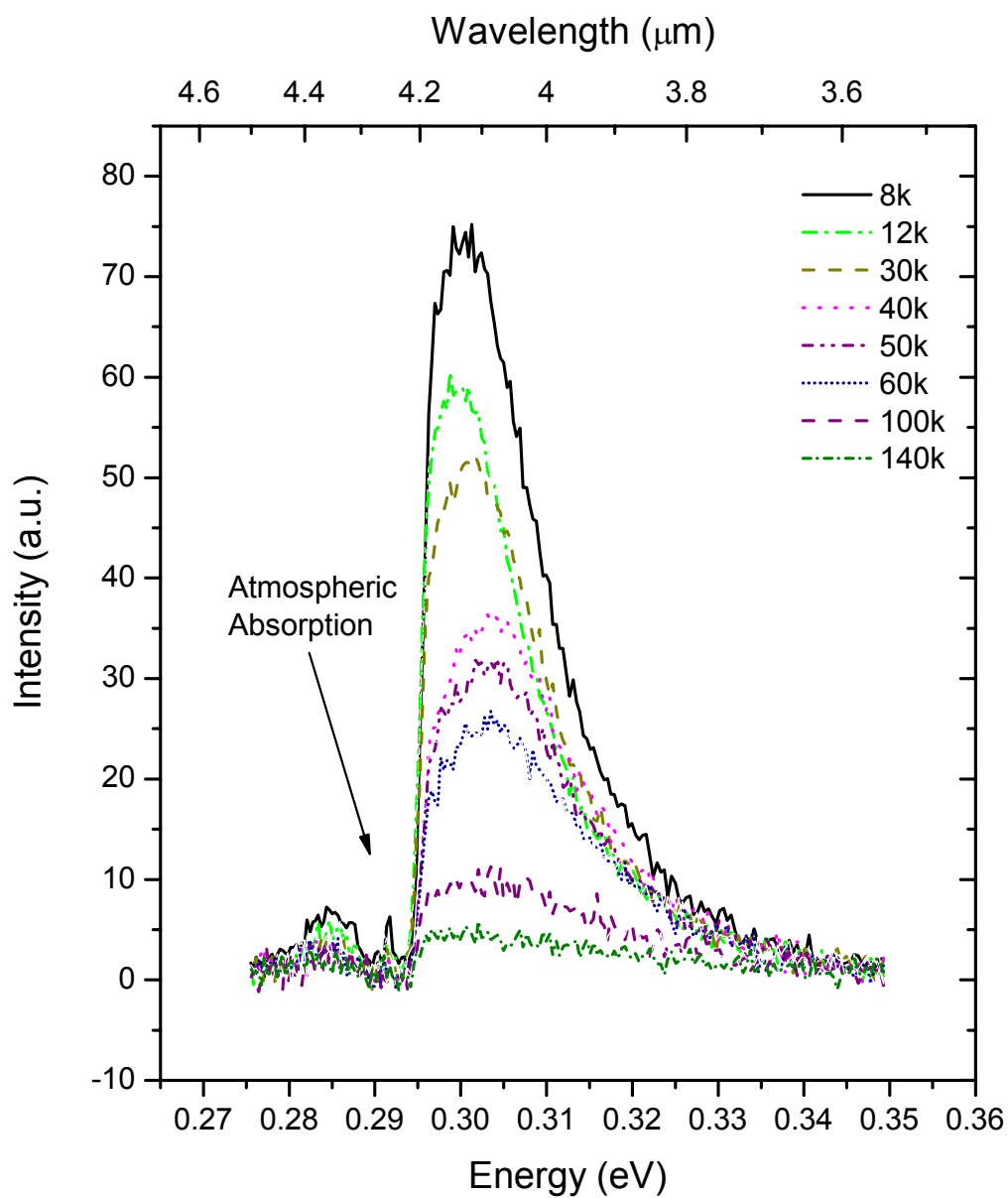
Figure 4.2. Sample R0-62 intensity as a function of energy at varying temperatures. The temperature resolution is 4K. The wavelength resolution is 5nm and the energy resolution is 8. meV. This plot clearly shows that E_g varies as a function of temperature. Also shown is the atmospheric absorption in the 2.8-2.95eV range.
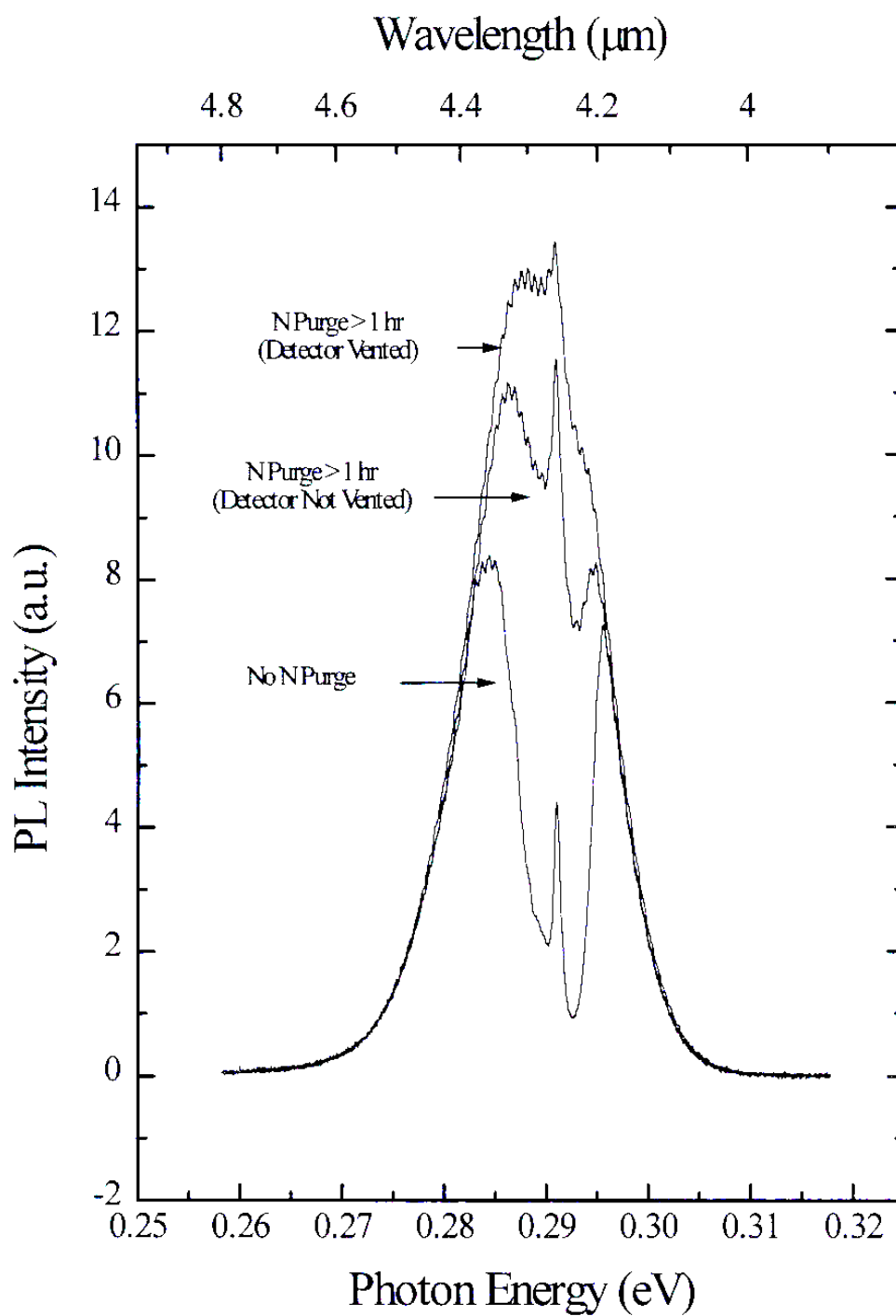
Figure 4.3. PL spectra showing the effects of a N_2 purge on reducing the CO_2 absorption at the wavelengths of interest (Marciniak, 1995: 5-19).

4.1.1 Temperature Variation

In bulk semiconductors, the bandgap changes as a function of temperature primarily due to a change in lattice constant with temperature. The effects of temperature on E_g follow the Varshni equation, Eq (4.1). The Varshni equation is dependent upon the E_g at 0K, denoted as $E_g(0)$, and the empirical Varshni parameters α and β.

$$E_g(T) = E_g(0) + \frac{\alpha T^2}{\beta + T} \tag{4.1}$$

Figure 4.4 shows the E_g dependence on temperature for bulk semiconductor material (Marciniak, 1995).

Plotting the radiative transitions in a QW sample at various temperatures indicates whether they also follow the Varshni equation. Figure 4.4 shows the E_g dependence on temperature over the range 8- 140 K for the sample set used here. Comparing the data collected with the InAs and $InAs_{0.05}Sb_{0.95}$ curves leads to the conclusion that both type-I and type-II samples appear to follow the Varshni equation. Type-I materials follow the Varshni equation much more strongly than type-II materials. The rise and then decrease of E_g with temperature in type-II materials prompted a modeling effort described later in this chapter. There is also an apparent discrepancy between the tight and diffuse waveguide and modeling will be used to analyze this.
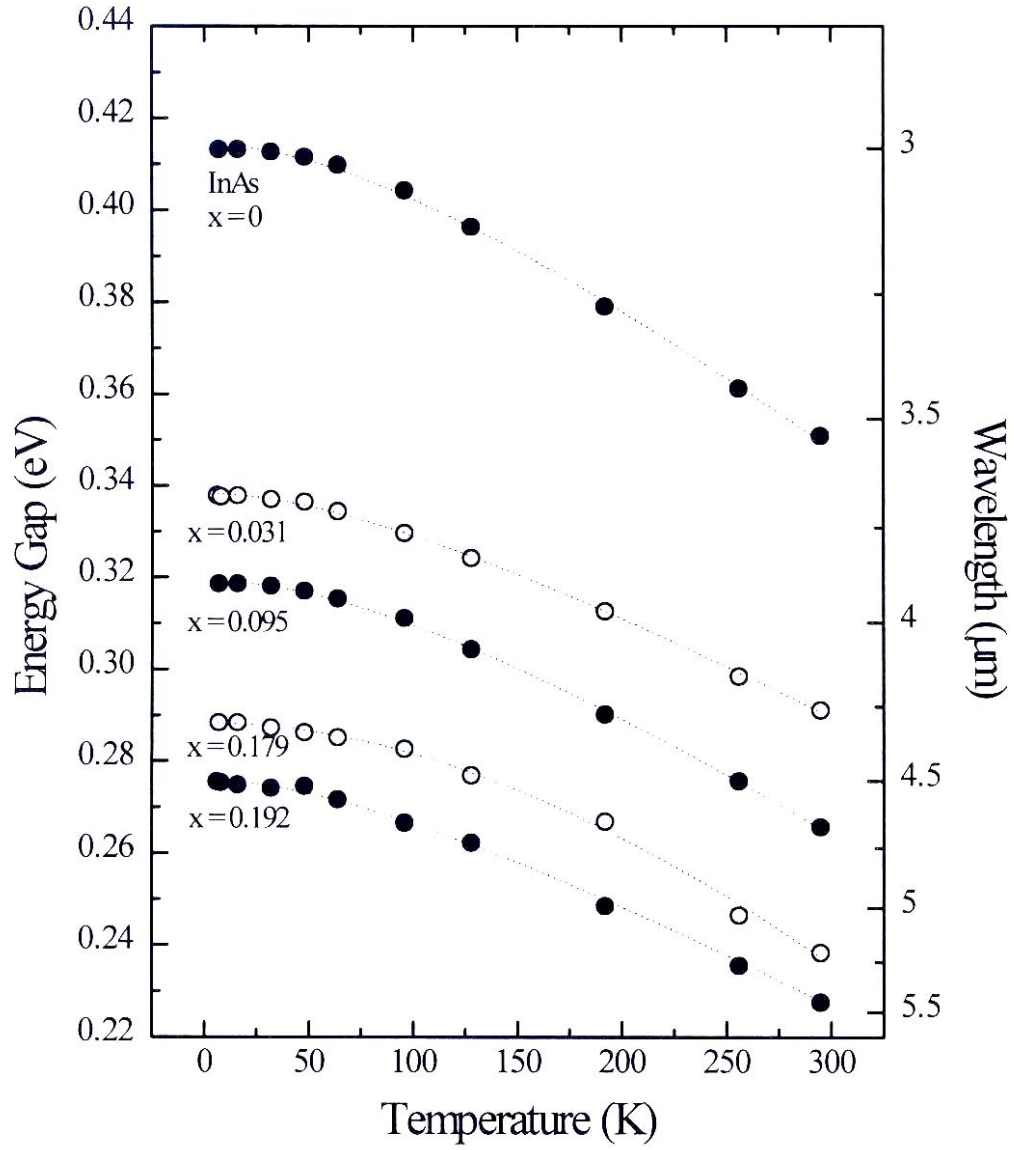
Figure 4.4. Temperature-dependence of the energy gap for epitaxial indium-arsenide-antimonide ($InAs_{1-x}Sb_x$) was measured. The dashed lines are a least squares fit of the Varshni equation to the data (Marciniak, 1995: 6-21).
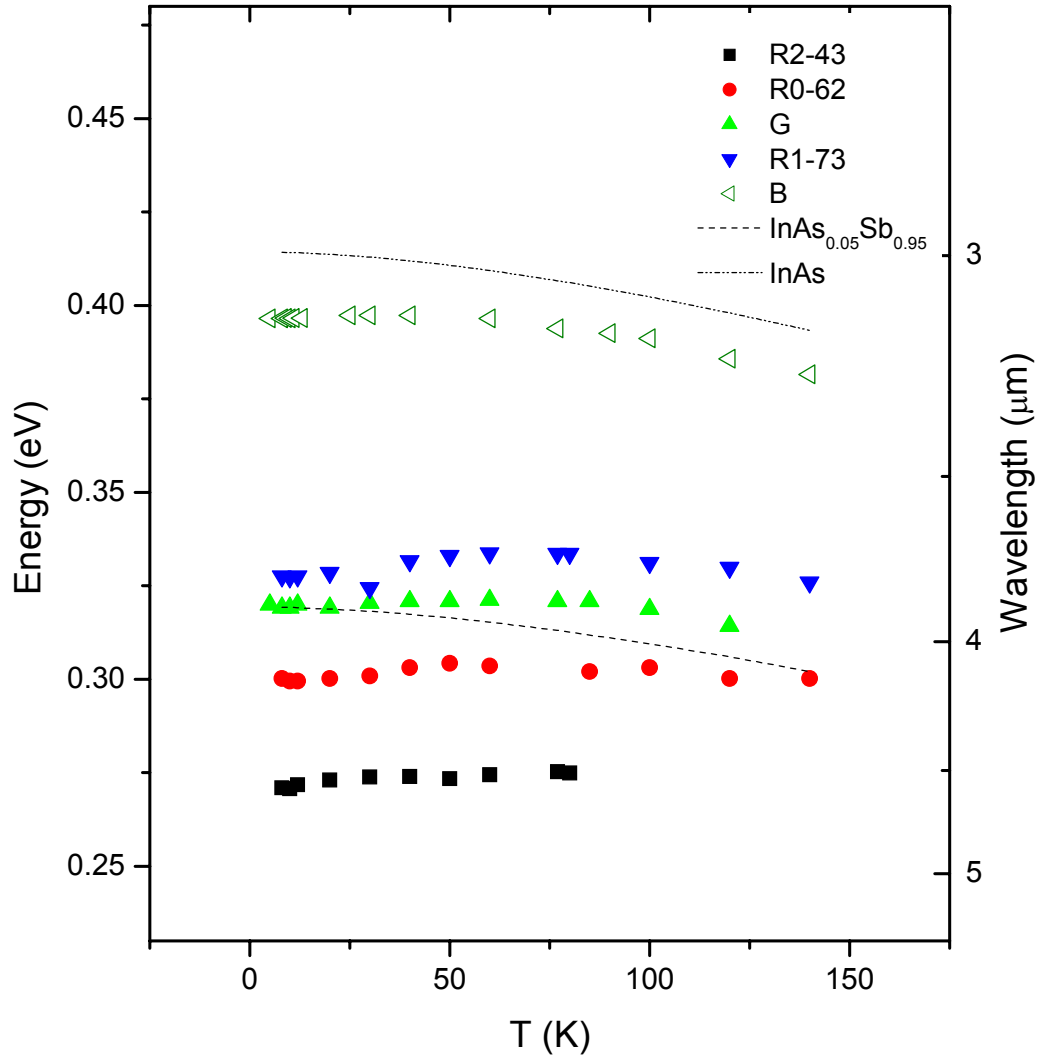
Figure 4.5. Comparison of the Varshni equation to E_g-as-a-function-of-T measurements in type-I and type-II semiconductor material. The type-I sample is represented by a hollow triangle and the type-II materials are represented by filled in symbols. The dashed lines are curves of the Varshni parameters in bulk semiconductor material, specifically InAs and $InAs_{0.05}Sb_{0.95}$.

4.1.2 Varying Excitation Power

Varying the excitation power and fitting the high energy side of the intensity-versus-energy/ wavelength curve with an exponential curve will yield time averaged carrier temperatures (T_c) as shown in Figure 4.6 (a). The T_c plots are shown in Figure 4.7. The T_c points are linearly fit to extract phonon energies from the line slopes. Another way to extract T_c is to plot the intensity at a given energy data as a function of temperature on a semi-log plot and fit the high energy side of the curve with a straight line as shown in Figure 4.6 (b). The slope of the line gives the T_c according to Eq (4.2). With simple manipulation T_c can be extracted with the same relation from the exponential.

$$T_c = \frac{-k_b}{m \log e} \qquad (4.2)$$

As seen in Eq (4.2), carrier temperature is dependent upon the slope of the line (m) and the Boltzman constant (k_b), as well as the constant –log e. T_c indicates how an excited electron gives off excess energy as it relaxes to the lowest point in the conduction band.

A higher T_c implies electrons are being excited higher into the conduction band. The higher an electron is in the conduction band the more energy it must give up before it can recombine with a hole. A higher amount of energy being transferred corresponds to the higher energy longitudinal optical (LO) phonon. Less energy being transferred corresponds to a lower energy acoustical phonon. Comparing the slope of the T_c curve with a line having slope $-k_B/h\nu_{LO}$, where ν_{LO} is the LO-phonon energy (~29meV for InAs and InAsSb compositions), will indicate which type of phonon the electron gives its

32

energy to (Marciniak, 1995: 7-43). When the slope of the T_c curve is approximately

equal to $-k_B/h\nu_{LO}$, the majority of the energy that the electrons transfer to the lattice is to

the LO-phonon. If the slope is less than the LO-phonon energy, the sample is in a mixed

regime of acoustical and optical phonons, or just the acoustical phonon regime. Figure

4.8 shows Shah's curve of T_c versus excitation power (Shah, 1978:45). The straight line

is a line with a slope equal to the LO-phonon energy in GaAs. The majority of the data

points lying upon the line indicates that the GaAs is in the optical phonon regime. If the

majority of the points corresponded to a line with a slope equal to the acoustical phonon

the GaAs would be in that regime. The samples in this experiment all lie on a line

corresponding to the high excitation power portion of Figure 4.8.

Figure 4.7 shows the carrier temperature as a function of excitation power for the

samples from which it could be extracted. Sample G has a phonon energy ($h\nu_{ph}$) of 100

meV, R0-62 has an $h\nu_{ph}$ of 81.29 meV, and sample R1-73 has a $h\nu_{ph}$ of 50 meV. These

values indicate that the carrier cooling is in the optical phonon regime but that the phonon

electron interaction is most likely not the primary method of electron energy transfer.

PL data for the samples from which T_c could not be extracted are shown in Figure

4.9. The linearity of the high-energy side of the sample B curve, Figure 4.9 (a), prevents

T_c extraction for that sample. T_c of sample R2-43, Figure 4.9 (b), could not be extracted

because emissions on the high-energy side of the curve are absorbed by CO_2 and there is

an extremely low signal-to-noise ratio.
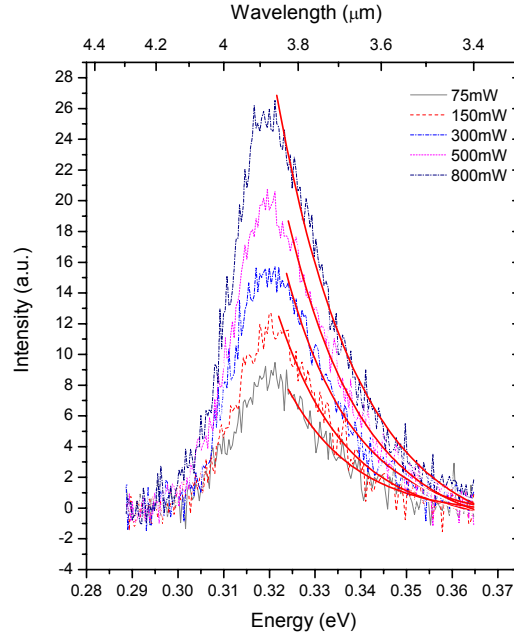
(a)
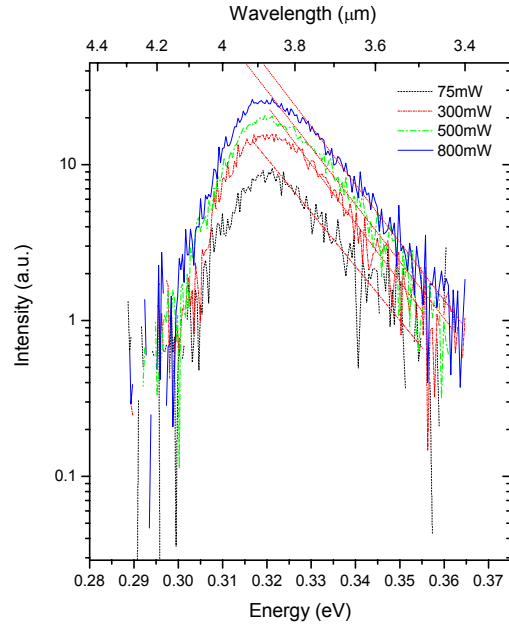
(b)

Figure 4.6. Exponential fitting to the high energy side of the intensity as a function of energy curve is used to calculate the T_c of sample G. T_c can also be extracted from a linear fit to a semi-log plot. The data from Sample G illustrates how the semi-log line fit is a more imprecise method due to the noise at the end of the collected spectrum and the slope's dependence on where the endpoints are chosen.
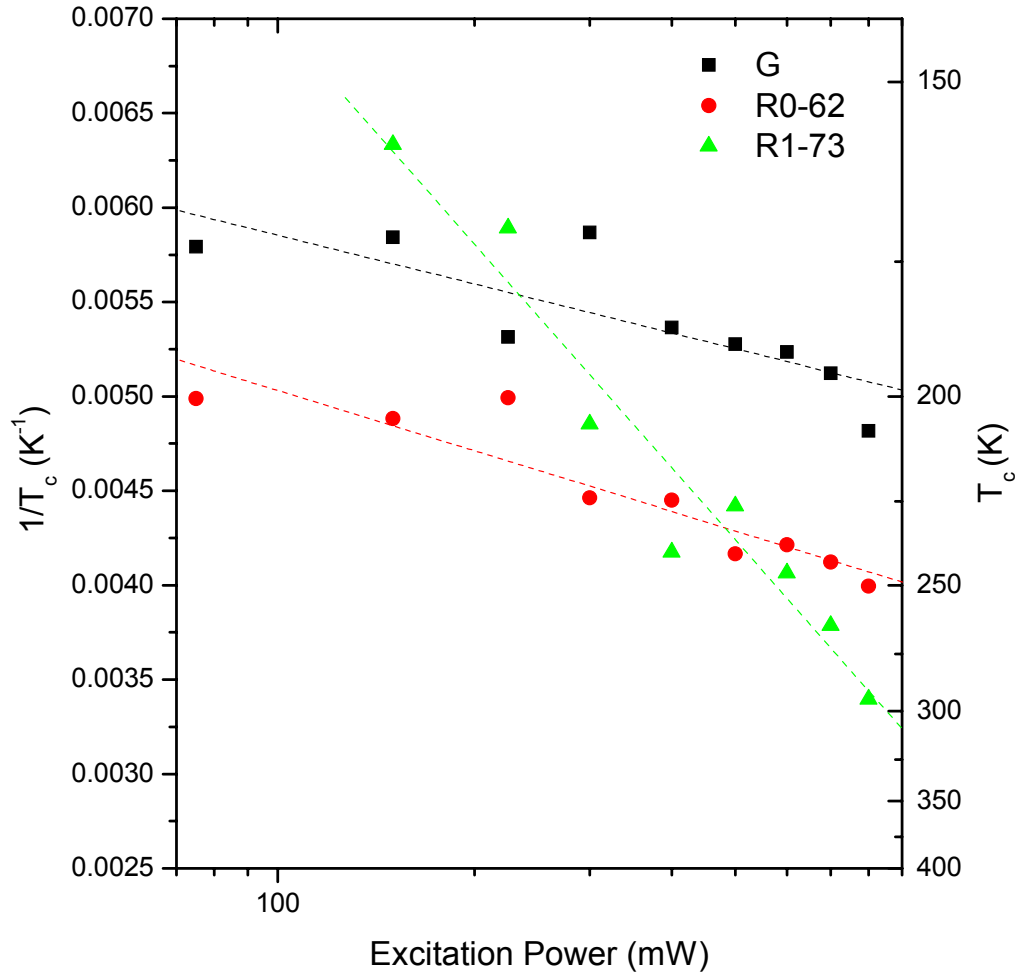
Figure 4.7. Inverse carrier temperature as function of excitation power for samples R0-62, R1-73 and G. The relative linearity of these plots indicates that the free carriers are giving off energy to LO-phonons. The dashed lines are a least squares linear fits to the data points with slopes -0.00106, -0.00393, and -8.59635 x 10^{-4} for samples R0-62, R1-73 and G respectively. The slopes of these lines indicate how the free carriers transfer energy to the lattice.
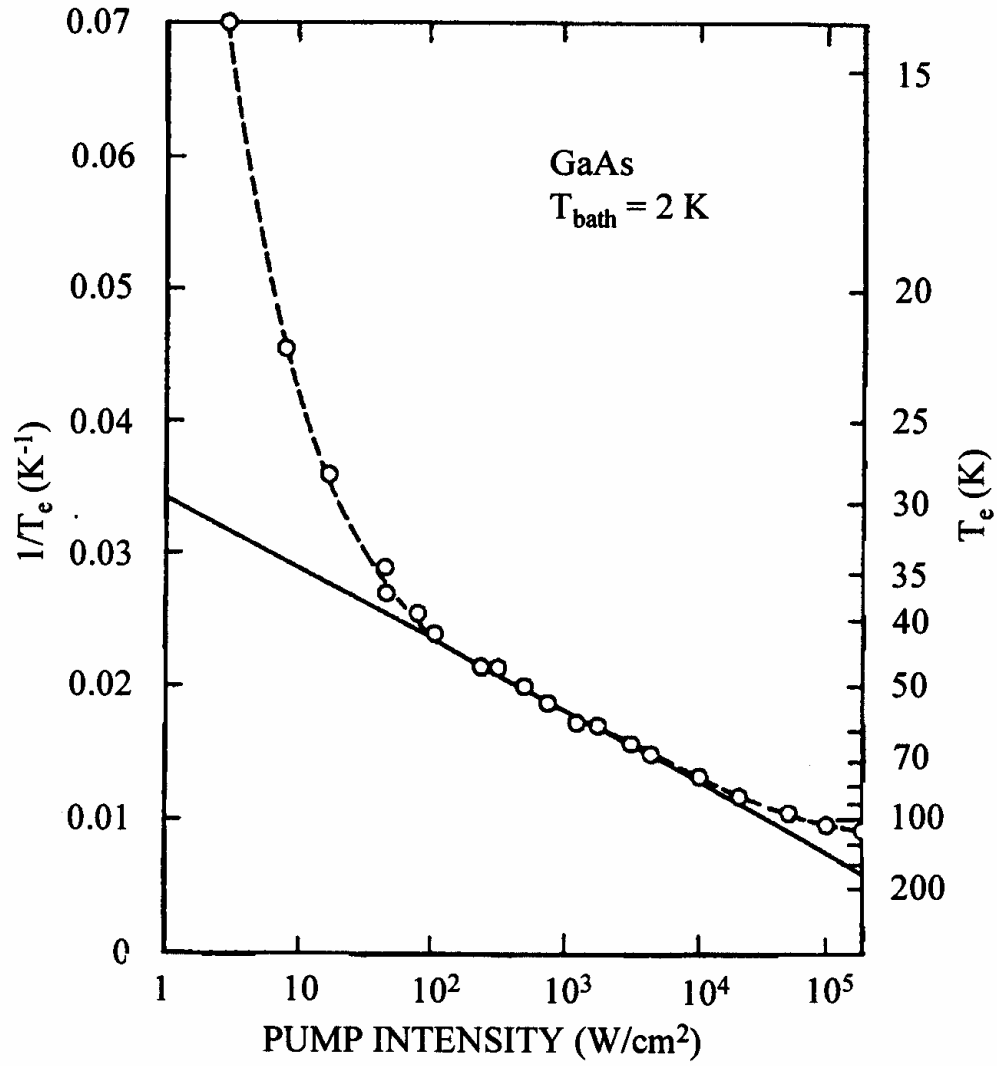
Figure 4.8. $1/T_c$ as a function of excitation intensity for GaAs at 2 K. The points are experimental data and the solid line corresponds to a slope of $-h\nu_0/k_B$ where $h\nu_0$ is the phonon energy. (Shah,1978:45)
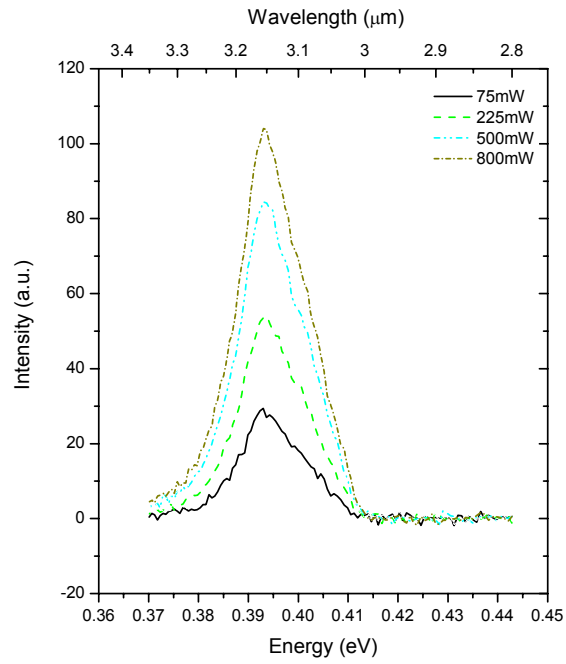
(a)
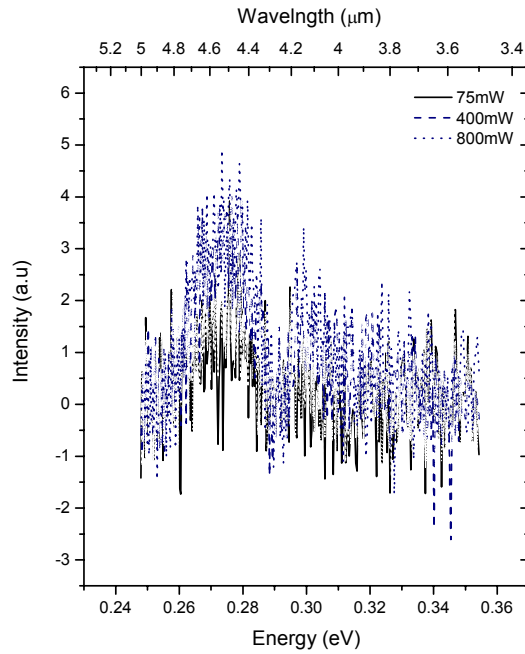
(b)

Figure 4.9. (a) Shows how T_c could not be extracted from sample B because of the linearity that dominates the high energy side of the curve. (b) T_c could not be extracted from R2-43 because of the low signal to noise ratio.

The radiative efficiency of each sample is obtained by integrating the area under the PL intensity-versus-excitation-photon-energy curve, as a function of excitation power. For the R0-63 and R1-43 curves, the region absorbed by atmospheric CO_2 was accounted for by fitting the curve to an exponential and using values of the exponential fit in those regions. Figure 4.10 shows integrated emission as a function of excitation power for all the samples. A higher slope indicates a higher efficiency. Sample B is clearly more efficient than the type-II samples. The tight and diffuse waveguide samples have the same active region and should therefore have the same efficiency. In Figure 4.11, the data for the tight waveguide (R0-62) and the diffuse waveguide (R2-43) coincide fairly well for excitation powers from 75-700 mW. The leveling off of R2-43 with higher excitation power indicates saturation in a region where R0-62 is still linearly rising. A slightly smaller quantum-well width in R2-43 might result in it becoming saturated more quickly than R0-62, and some discrepancy in the well widths is an expected result of the growth process.

4.2 Modeling

If two materials have the same active region, they should exhibit the same emission properties provided they are both at the same temperature and excited with the same excitation source. The fact that sample R0-62 has an AlGaAsSb cladding should not influence the emission because this layer is a dielectric and will not affect the excitation photons.

38
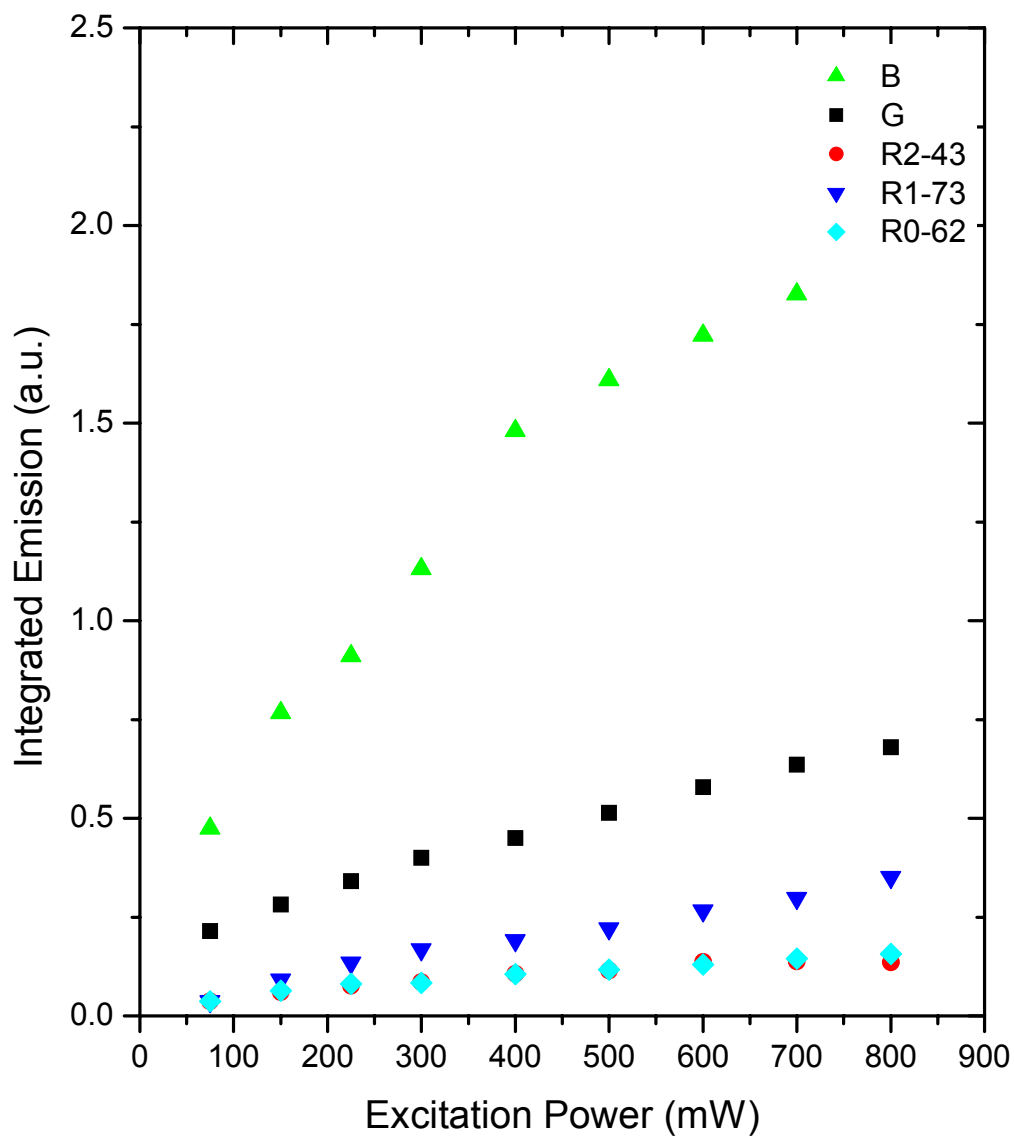
Figure 4.10. Integrated emission as a function of excitation power for all samples. The sample temperature is 80 K. The resolution of the excitation power is 2 mW.
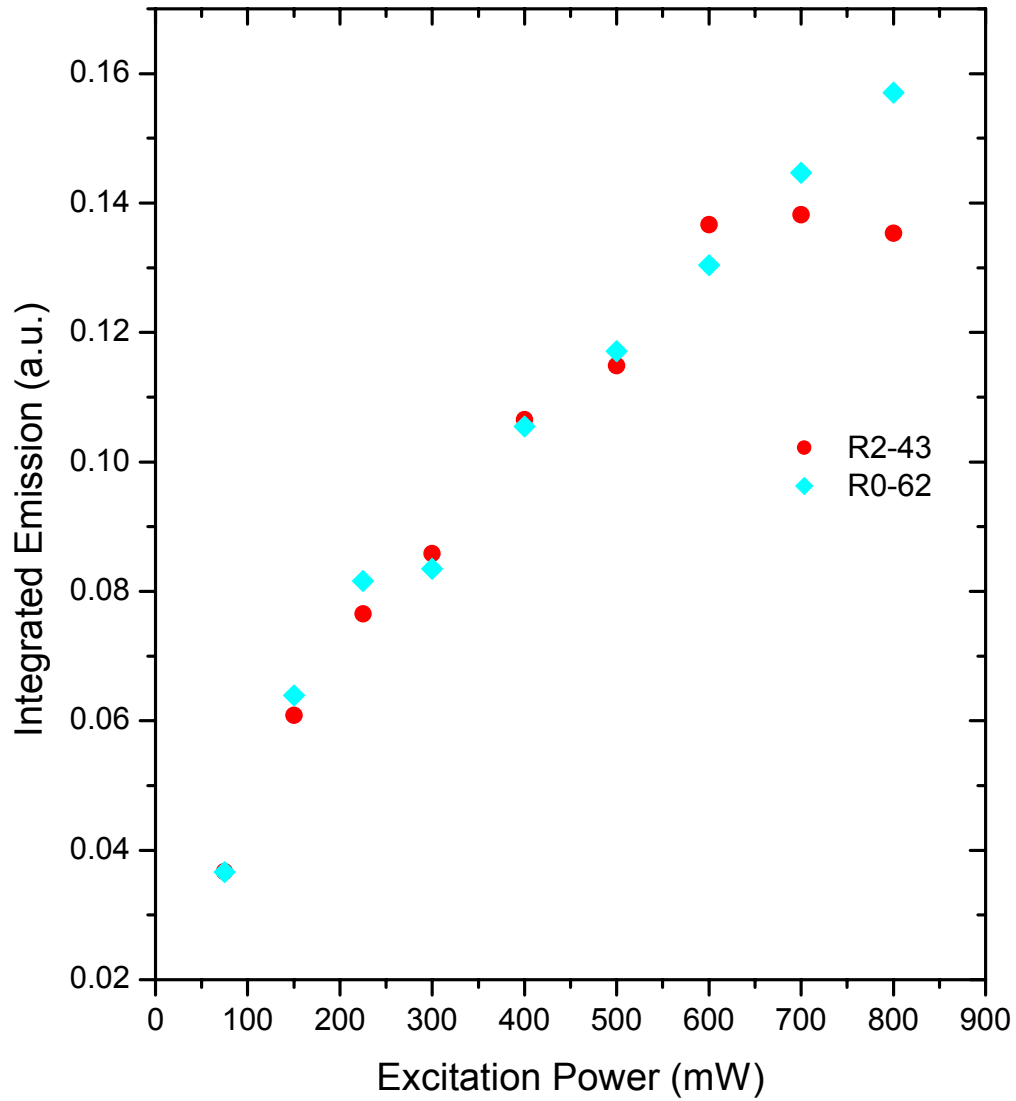
Figure 4.11. Plot of the efficiency curves for the tight waveguide sample, R0-62, and the dilute waveguide sample, R2-43, with nominally the same active regions. Samples are both at 80 K and excitation power resolution is 2 mW.

The cladding layer likewise should not affect the thermal properties of the active region. What causes the differences in efficiency and E_g as a function of temperature in R0-62 and R2-43 then? Modeling this active region is one way of trying to understand what is happening.

A commercially available modeling code written by Ram- Mohan was used for this effort. To utilize the code, the material parameters of ternary and quaternary compositions were linearly interpolated from those of the binary materials. The code itself and *Band parameters for III-V compound semiconductors and their alloys*, by Vurgaftman, were the primary sources of the parameters for the binary compositions. The values for E_g and lattice constant were altered to represent the effects of temperature where appropriate. These values were obtained from the Mathematica code given in Appendix A. The difference between linear interpolation and an altered interpolation method, utilizing Eq (4.3), is shown in Figure 4.12. Eq (4.3) is derived from assumption that $E_{g3}(T) = x(E_{g1}(T)) + (1-x)(E_{g2}(T))$ where x is the mole fraction of one of the binary constituents. By creating a table of E_{g3} points at various temperatures and fitting those points with a Varshni equation, the empirical Varshni parameters for the ternary or quaternary compositions were determined. For samples R0-62 and R1-43 $\alpha = -0.000401165$ and $\beta = 143.27$.

$$E_{g3}(T) = x\left(E_{g1}(0) + \frac{\alpha_1 T^2}{\beta_1 + T}\right) + (1-x)\left(E_{g2}(0) + \frac{\alpha_2 T^2}{\beta_2 + T}\right) \qquad (4.3)$$

Figure 4.12 (a) shows that the difference between linear interpolation and the altered method for the ternary composition is a constant. Figure 4.12 (b) illustrates that the

difference is much more pronounced in a quaternary composition. For this reason, the altered interpolation was used for the input file into the computer code.

The input for the **femb** code included composition of a ternary compound created from binary compositions, as well as the sample temperature of the modeled ternary sample. The model produced a table of band offsets used to generate band diagrams, like Figure 4.13, and lists of eigenvalues used to compare predicted possible transition energies with luminescence energies in the data.

The variation of lattice constant with changing temperature on the band diagram is negligible when compared to variations with temperature of E_g. Figure 4.14 shows an expanded view of the upper right corner of the conduction band well as a function of temperature. The slight bowing of the E_g-as-a-function-of-T curve in Figure 4.5 in type-II materials was initially thought to be a result of well-width variations produced from lattice constant variations with temperature, but the negligible change of quantum well width with temperature makes this unlikely.

The model predicts an E_g-as-a-function-of-T curve that follows the Varshni equation. Figure 4.15 shows the modeled curve along with the actual data. The predicted curve is closer to the observed R2-43 data in energy, but neither R2-43 nor R0-62 follow the prediction closely. The discrepancy between the model and the data might be accounted for with well-width variations introduced in the growth process, but was untested in the modeling. The cause of the differences might also be a result of linear interpolation of the material parameters. Appendix A shows the large discrepancy in linearly interpolated and actual Varshni parameters. Other parameters might change as drastically with temperature as the Varshni and E_g parameters.
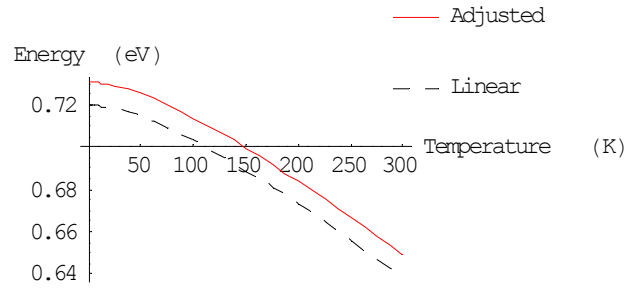
(a)
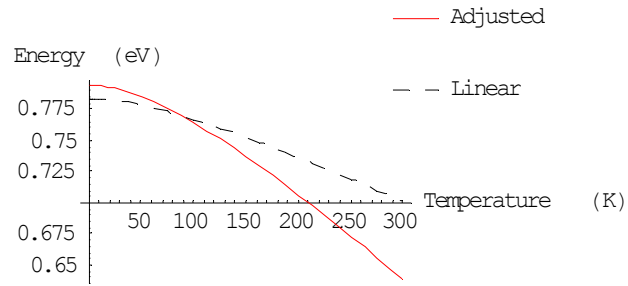
(b)

Figure 4.12. (a) shows the difference in the ternary composition between a linear interpolation of the Varshni parameters and an altered interpolation of the Varshni parameters given by Eq (4.3). (b) shows the difference in the quaternary between a linear interpolation of the Varshni parameters and an altered interpolation of the Varshni parameters given by Eq (4.3)
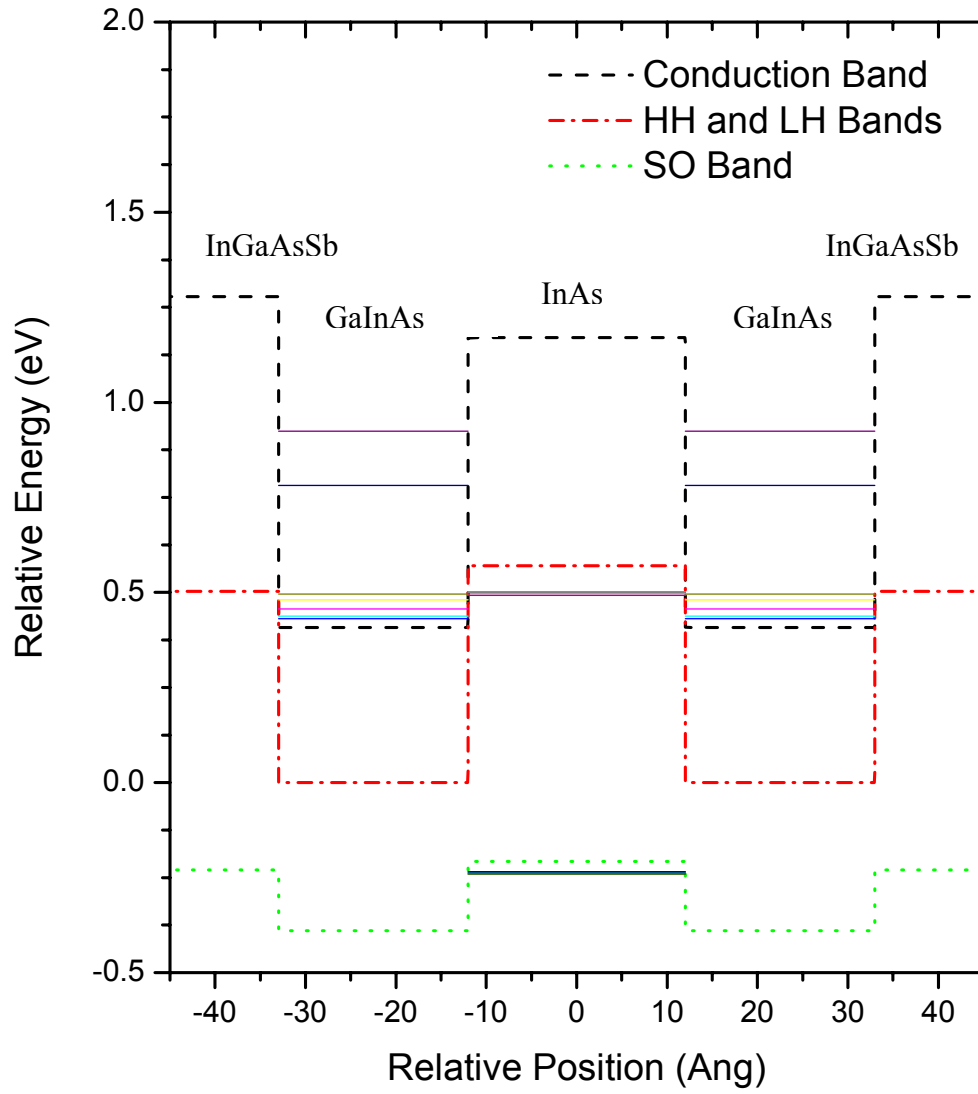
Figure 4.13. Band diagram for the active region of samples R0-62 and R2-43. The valence band offsets are calculated from GaSb. The material temperature is 77 K in this diagram.
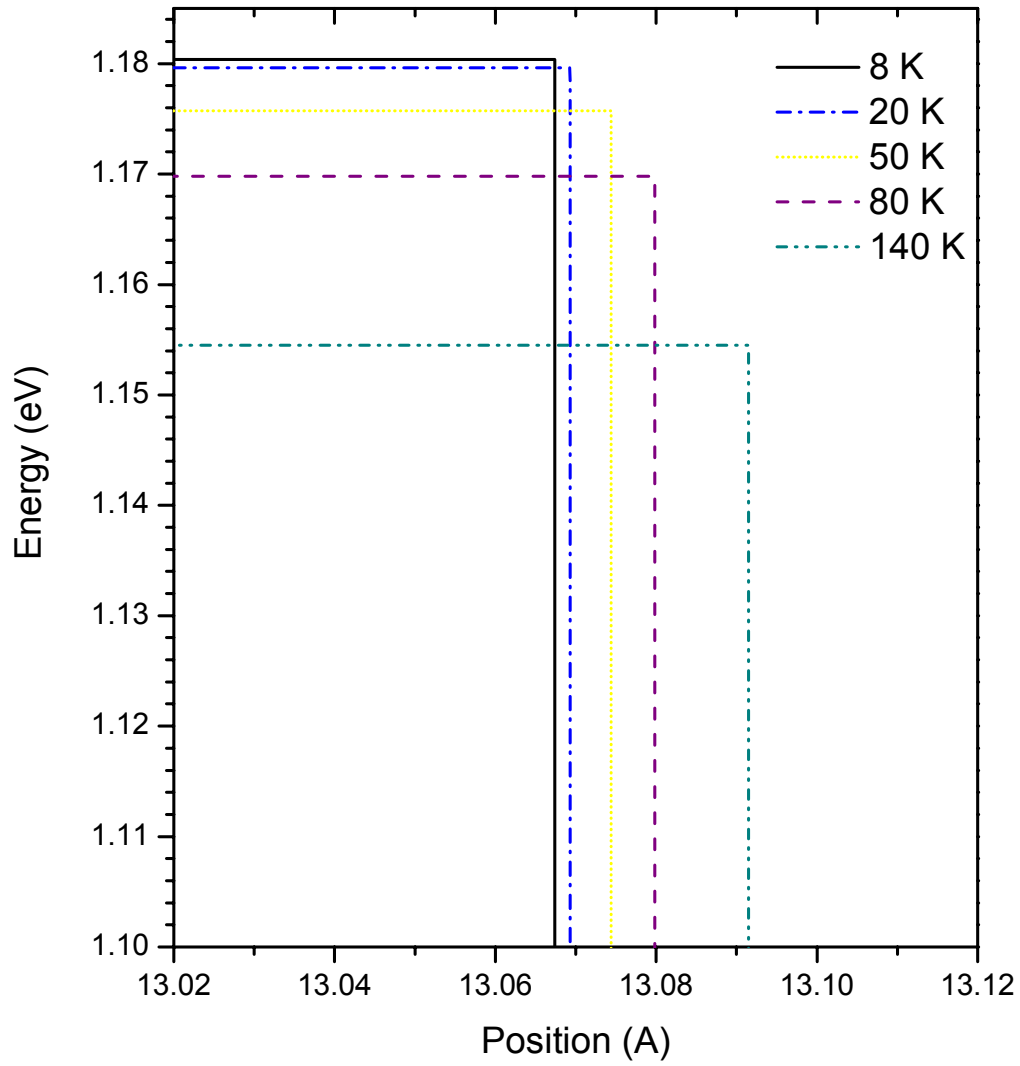
Figure 4.14. Diagram for samples R0-62 and R2-43 of the upper right (highest energy, highest relative distance) corner of the conduction band well as a function of temperature.
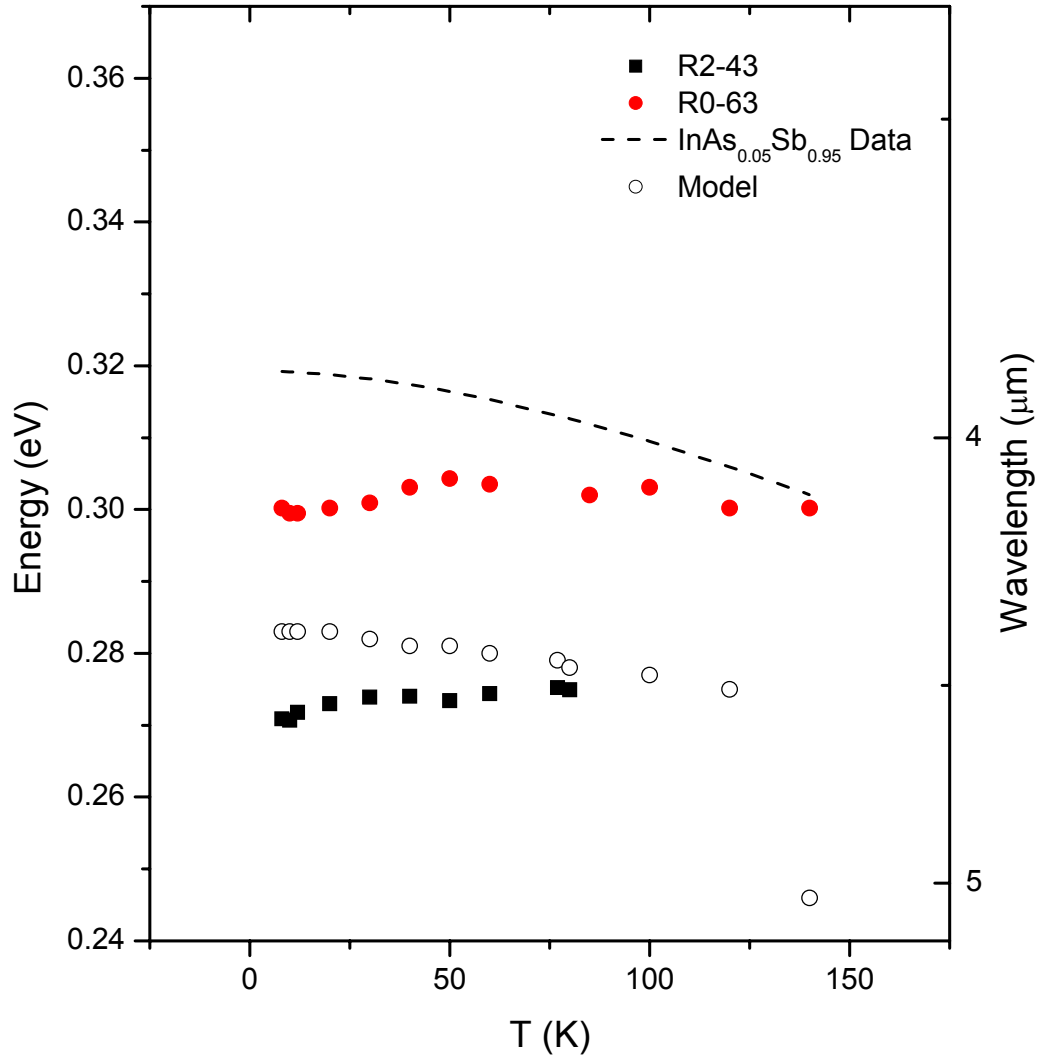
Figure 4.15. The hollow circles are the predictions from the **femb** code for $E_g(T)$ for sample R0-62 and R2-43. The solid shapes are experimental data points for R0-62 and R2-43. The dashed line is an experimental curve for bulk InAsSb.

4.4 TRPL

The TRPL experiment did not work well enough to extract information. However, as shown in Figure 4.16, the attempt to achieve frequency upconversion with this experiment was successful. The rise in intensity that corresponds to 0 ps on the curve is the point at which the PL and the pump beam are mixing at their maximums. The decrease in intensity at increasing time delay is indicative of the decay of the PL pulse as free carriers recombine and their number decreases. Unfortunately, the signal-to-noise ratio for this experiment could never be improved from that shown in this figure. A possible explanation for this error is misalignment somewhere on the optics table.
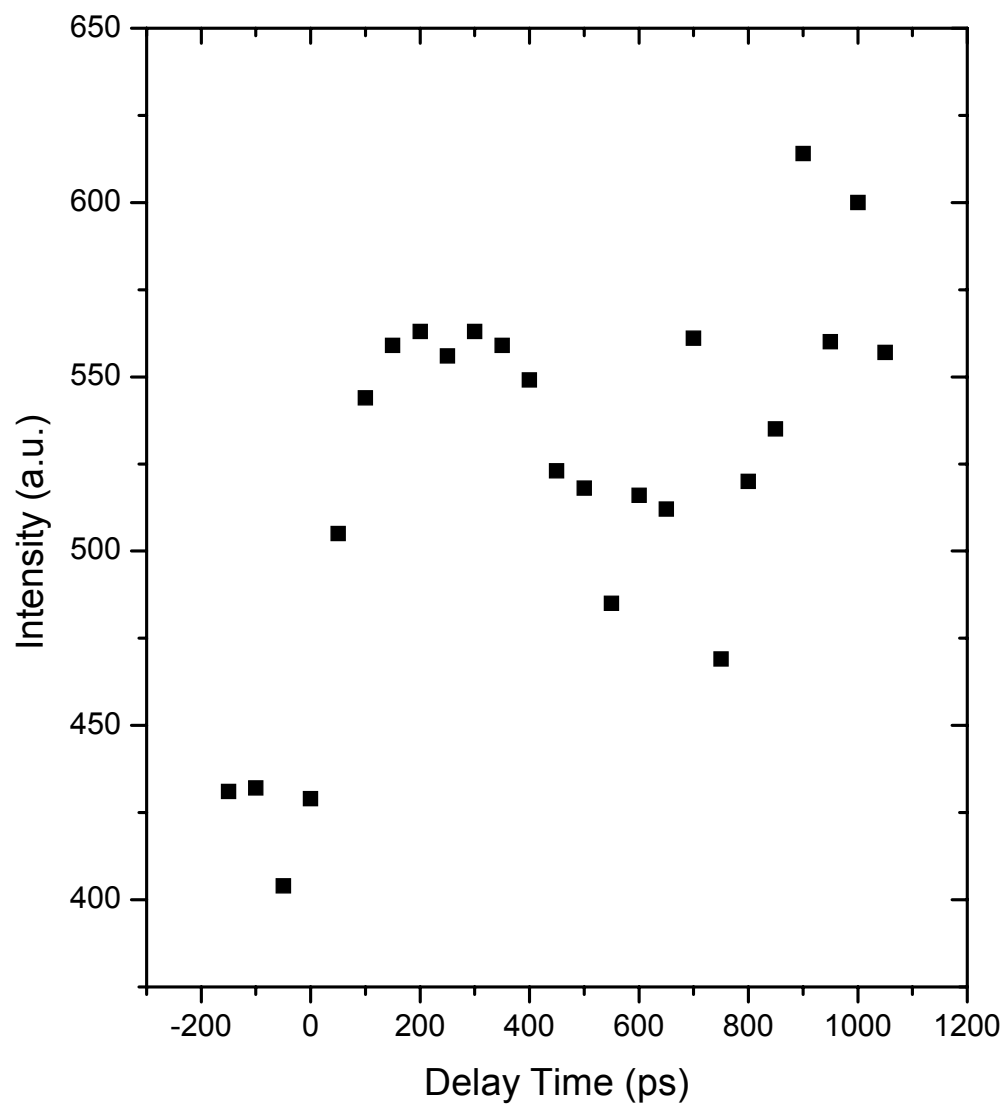
Figure 4.16. TRPL curve that demonstrates that upconversion was achieved. The appearance of noise at 700 ps delay could not be removed.

5. Conclusions and Recommendations

The current and rising IR-missile threat is forcing the Air Force to change its tactics and operations in order to protect aircrews. This same threat is also creating the requirement for a lightweight IR-missile counter-measure system. IR missiles work in the 3-5-μm transmission window and any laser to defeat these missiles must exploit this same window. Semiconductor lasers are lightweight, efficient and reliable, making semiconductor lasers an ideal solution to the IR-missile problem. Antimony-based MQW semiconductor structures can be fabricated into lasers that will propagate in the required atmospheric transmission window. By characterizing these samples with time-averaged PL experiments, computer modeling to predict their behavior and TRPL experiments to characterize their temporal performance, better structures can be found. This will lead to making an IR-counter-measure laser device that can be mounted on fighter-sized aircraft a reality.

This experiment performed a PL study to characterize E_g response to temperature. Bulk semiconductor material follows the Varshni equation and the E_g response to temperature can be predicted with it. Type-I structures were shown to follow the Varshni equation well, whereas, type-II structures deviated from the Varshni equation with a rise and then a decrease in E_g as temperature increased. This rise was seen in all the type-II samples and led to a modeling effort of type-II structures. Also, when examining E_g response to temperature, the effects of a waveguide cladding were examined. The sample with the cladding, which corresponds to the tight waveguide, differed from the sample without the cladding, which corresponds to the dilute waveguide. The expectation was that the two materials would exhibit the exact same characteristics because the active

regions are the same. The active region is the only location were any affects that effect luminescence should be taking place.

Varying the excitation power incident upon the sample during the PL study provided information on T_c and radiative efficiency. The carrier temperature could only be extracted from two of the five samples. Low signal-to-noise ratio and a non-exponential curve prevented the other two samples from being characterized in this manner. The T_c values that were extracted both indicated a higher phonon energy than the published optical phonon energy of ~29 meV, leading to the conclusion that both samples were in the optical phonon regime.

Efficiency was determined by integrating the area under the PL curve as excitation power was varied. The integrated emission-as-a-function-of-excitation-power curves indicated that the type-I sample is more efficient than the type-II samples. The efficiencies of the tight-waveguide and diffuse-waveguide samples were different. The diffuse waveguide was saturated in a temperature regime where the tight waveguide was still linearly efficient.

The difference in efficiency combined with the difference of the type-II structures from the Varshni equation led to the utilization of a commercially available model. The model was set up with material parameters linearly interpolated from binary materials. The highly temperature-dependent variables of Varshni parameters, E_g, and lattice constant were found using Mathematica given code in Appendix A. The discrepancies in the type-II material from the Varshni equation were not a consequence of changing lattice constant with temperature, or a result of changing bandgap according to the model. A better understanding of the model would be very useful to future work.

TRPL resulted in a working frequency upconversion experiment that could not be optimized enough to gather useful data. There appears to be a systematic error that indicates an alignment problem. This alignment issue was not solved in the time allotted for TRPL.

Improved alignment of the TRPL experiment and further understanding of the computer model would both be possible with more time. The computer model should be examined with a single quantum well to establish the variance of the input parameters. Progression to a type-I MQW sample would provide insight into the way the model accounts for interaction between electron and hole wells. Finally, the model would be understood enough to make excellent use of its computational powers to examine type-II materials. The cladding layers should be modeled with the type-II structures to see if the model predicts any of differences observed experimentally that may be caused by the cladding layer. Thickness of the sample layers should also be varied in the model to determine if differences in variations inherent in the growth process dramatically affect the performance of a sample. Figure 5.1 shows the recommended variations to the model's input parameters. The variations are combinations of changes of 1-2 monolayers in well-width, up to a 10% variation in valance band offset for the quaternary composition, and up to a 10% variation in the quaternary composition. The straight arrows are the parameters that are well known, the dashed arrows are the recommended variations for future analysis. The model should be used to run "test" materials before they are grown to ensure that only the best samples are actually examined in the laboratory.

An optimized upconversion experiment would provide insight into the temporal response of the PL signal. This can be accomplished by proper alignment. The recombination coefficients could then be determined and the time-dependent T_c could be compared to the time-averaged T_c obtained during PL. This would provide insight into thermalization processes occurring in the sample material.

The goal of this experiment was to characterize a set of type-I and type-II samples, and provide insight into which materials would best meet the needs of the Air Force for use in an IR-missile countermeasure system. The effects of temperature and excitation power were determined, and a model of a type-II structure was examined. A step closer to the end product was made, but more work is needed to get to a defensive capability in the field.
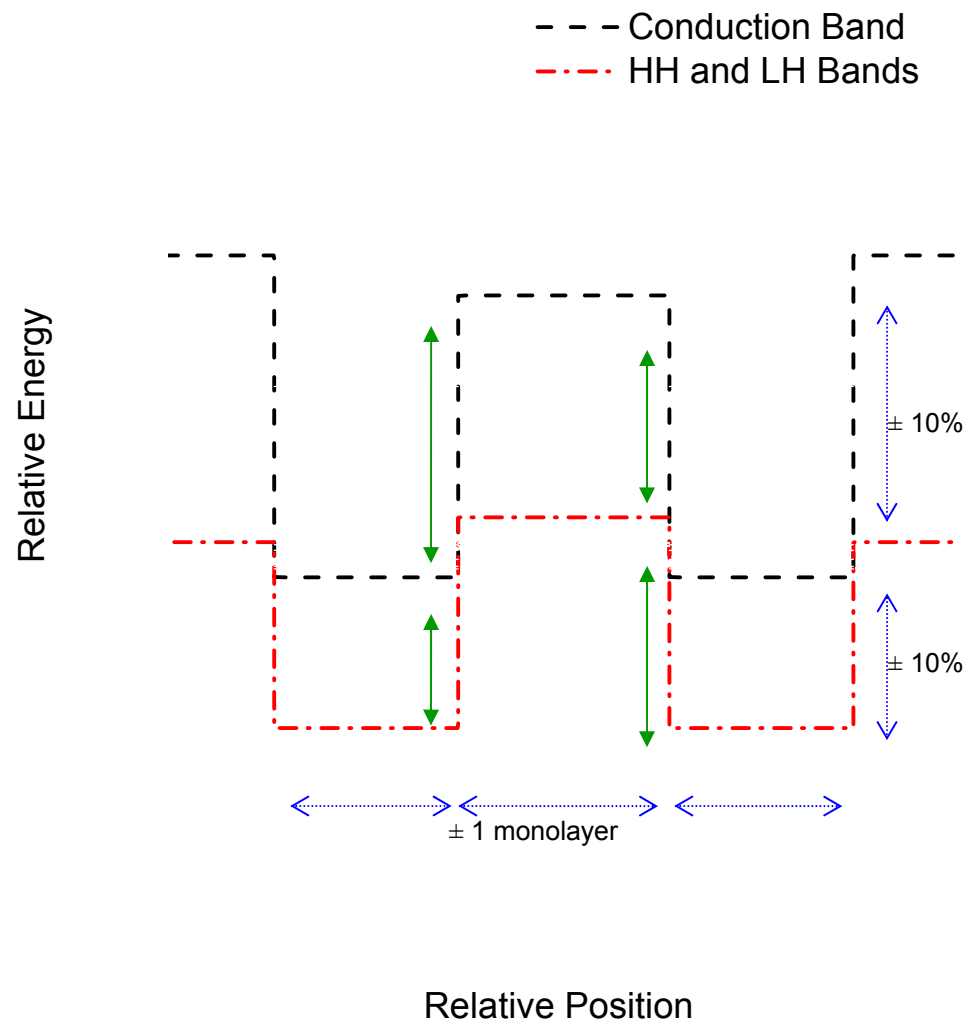
Figure 5.1. Recommended future modeling work. The parameters that should be changed and by how much.

```
<< Graphics`Legend`
```

Mohan's Data

```
GaSb := {.812, 23.844, .76, 0, 13.4, 4.7, 6.0, 3.18, .13, -7.5,
   -.8, -2, -4.7, 0, 8.842, 4.026, 4.322, 14.5 10⁻³, 0, 570, 4.8,
   6.09593, -.03, .417 10⁻³, 140}
```

$$GaSbo = GaSb[[1]] + \frac{GaSb[[24]] * 77^2}{GaSb[[25]] + 77}$$

```
0.823394
```

```
InSb := {.235, 23.154, .81, 0, 34.8, 15.5, 16.5, 14.76, .15,
   -6.94, -.36, -2, -4.7, 0, 6.847, 3.735, 3.111, 16.5 10⁻³, 0,
   474, 4.9, 6.47937, 0, .32 10⁻³, 170}
```

$$InSbo = InSb[[1]] + \frac{InSb[[24]] * 77^2}{InSb[[25]] + 77}$$

```
0.242681
```

```
GaAs := {1.5194, 22.521, .341, 0, 6.98, 2.06, 2.933, 1.2, .04,
   -7.17, -1.16, -2, -4.8, 0, 12.21, 5.66, 6, 11.3 10⁻³, 0, 748,
   4.67, 5.65325, -.8, .5405 10⁻³, 204}
```

$$GaAso = GaAs[[1]] + \frac{GaAs[[24]] * 77^2}{GaAs[[25]] + 77}$$

```
1.5308
```

Building the Ternary

```
InGaSb[x_] := Table[(InSb[[i]] + ((GaSb[[i]] - InSb[[i]]) * x)),
   {i, 1, 25}]
```

```
Ternary := InGaSb[.84]
```

```
Ternary
```

```
{0.71968, 23.7336, 0.768, 0, 16.824, 6.428, 7.68, 5.0328, 0.1332,
 -7.4104, -0.7296, -2, -4.7, 0, 8.5228, 3.97944, 4.12824,
 0.01482, 0, 554.64, 4.816, 6.15728, -0.0252, 0.00040148, 144.8}
```

Building the Quaternary

```
InGaAsSb[y_] := Table[(Ternary[[i]] + ((GaAs[[i]] - Ternary[[i]]) * y)),
   {i, 1, 25}]
```

```
Quaternary := InGaAsSb[0.08]
```

```
Quaternary
```

```
{0.783658, 23.6366, 0.73384, 0, 16.0365, 6.07856,
 7.30024, 4.72618, 0.125744, -7.39117, -0.764032, -2,
 -4.708, 0, 8.81778, 4.11388, 4.27798, 0.0145384, 0,
 570.109, 4.80432, 6.11696, -0.087184, 0.000412602, 149.536}
```

Plotting the Linear Interpolation of the Ternary

$$E_g[T\_] := Ternary[[1]] - \frac{Ternary[[24]] \, T^2}{Ternary[[25]] + T}$$

```
Plot[Eg[T], {T, 0, 300}]
```
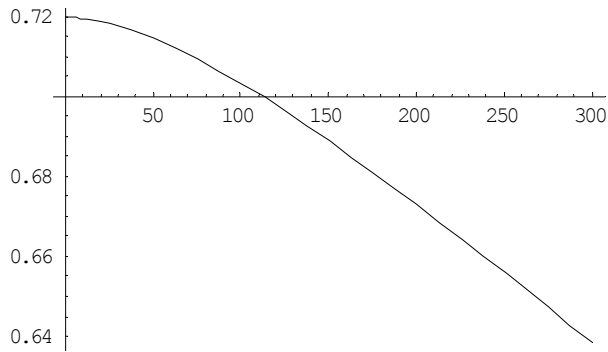
- Graphics -

$$En_g[T\_] := GaSbo\ .84 + InSbo\ .16 - \left(\frac{.16\ InSb[[24]]\ T^2}{InSb[[25]] + T} + \frac{.84\ GaSb[[24]]\ T^2}{GaSb[[25]] + T} \right)$$

```
Plot[{En_g[T], E_g[T]}, {T, 0, 300},
 PlotStyle → {RGBColor[1, 0, 0], Dashing[{0.05, 0.05}]},
 AxesLabel → {"Temperature (K)", "Energy (eV)"},
 PlotLegend → {"Adjusted", "Linear"}, LegendPosition → {.2, .1},
 LegendShadow → None, LegendSize → {.5, .5}]
```
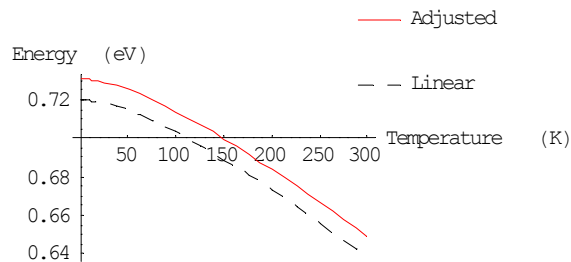

- Graphics -

Finding the Actual α and β Values for the Ternary

```
Data_3 = Table[{T, En_g[T]}, {T, 0, 300, 5}]
```

```
{{0, 0.73048}, {5, 0.730412}, {10, 0.730218}, {15, 0.729909},
 {20, 0.729496}, {25, 0.728989}, {30, 0.728395}, {35, 0.727722},
 {40, 0.726976}, {45, 0.726163}, {50, 0.725289}, {55, 0.724357},
 {60, 0.723373}, {65, 0.72234}, {70, 0.721261}, {75, 0.72014},
 {80, 0.718979}, {85, 0.717781}, {90, 0.716549}, {95, 0.715284},
 {100, 0.713988}, {105, 0.712664}, {110, 0.711313},
 {115, 0.709937}, {120, 0.708537}, {125, 0.707114},
 {130, 0.70567}, {135, 0.704206}, {140, 0.702723}, {145, 0.701221},
 {150, 0.699703}, {155, 0.698168}, {160, 0.696617}, {165, 0.695052},
 {170, 0.693472}, {175, 0.69188}, {180, 0.690274}, {185, 0.688656},
 {190, 0.687027}, {195, 0.685386}, {200, 0.683735}, {205, 0.682074},
 {210, 0.680402}, {215, 0.678722}, {220, 0.677032}, {225, 0.675334},
 {230, 0.673628}, {235, 0.671913}, {240, 0.670192}, {245, 0.668462},
 {250, 0.666726}, {255, 0.664983}, {260, 0.663233}, {265, 0.661477},
 {270, 0.659715}, {275, 0.657947}, {280, 0.656174}, {285, 0.654395},
 {290, 0.652611}, {295, 0.650821}, {300, 0.649027}}
```

<< Statistics`NonlinearFit`

NonlinearFit$\left[\text{Data}_3, (\text{GaSbo }.84 + \text{InSbo }.16) - \dfrac{\alpha\, T^2}{\beta + T}, \{T\}, \{\alpha, \beta\}\right]$

$0.73048 - \dfrac{0.000401165\, T^2}{143.274 + T}$

Ternaryo := 0.73048;

Plot$\left[\left\{\text{En}_g[T], 0.7304795608358365` - \dfrac{0.0004011649845616561`\, T^2}{143.27414819504622` + T}\right\},\right.$

$\{T, 0, 300\}\Big]$
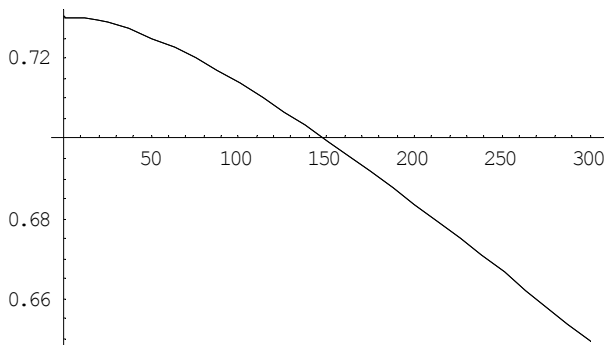
- Graphics **-**

Finding the α and β Values for the Quaternary

Energy$_g$[T_] := Ternaryo $.92 + \text{GaAso }.08 -$

$$\left(\dfrac{.92\, 0.000401165\, T^2}{143.274 + T} + \dfrac{.84\, \text{GaAs}[[24]]\, T^2}{\text{GaAs}[[25]] + T}\right)$$

Data$_4$:= Table[{T, Energy$_g$[T]}, {T, 0, 300, 5}]

NonlinearFit$\left[\text{Data}_4, (\text{Ternaryo }.92 + \text{GaAso }.08) - \dfrac{\alpha\, T^2}{\beta + T}, \{T\},\right.$

$\{\alpha, \beta\}\Big]$

$$0.794506 - \frac{0.000817475\ T^2}{171.682 + T}$$

```
f[T_] := 0.7945059486120997` - 0.0008174746783505516` T²
                               ────────────────────────────
                               171.68239833077624` + T
```

```
Q[T_] := Quaternary[[1]] - Quaternary[[24]] T²
                          ────────────────────
                          Quaternary[[25]] + T
```

```
Dimensions[Quaternary]
```

{25}

Redefining the Quaternary Input File

```
Plot[{f[T], Q[T]}, {T, 0, 300},
 PlotStyle → {RGBColor[1, 0, 0], Dashing[{0.05, 0.05}]},
 AxesLabel → {"Temperature (K)", "Energy (eV)"},
 PlotLegend → {"Adjusted", "Linear"}, LegendPosition → {.2, .1},
 LegendShadow → None, LegendSize → {.5, .5}]
```
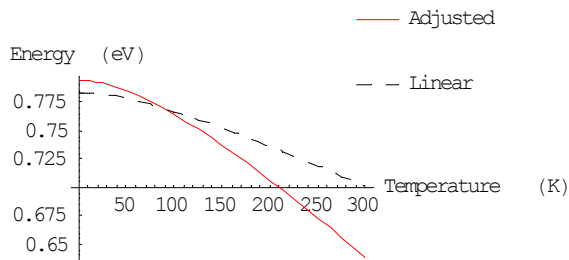

- Graphics -

```
InGaAsSbo = {0.794506, 23.636592000000004`, 0.73384`, 0,
    16.036479999999997`, 6.078559999999995`, 7.30024`,
    4.726176`, 0.12574400000000002`, -7.391168`, -0.764032`,
    -2, -4.708`, 0, 8.817776`, 4.1138848`, 4.2779808`, 0.0145384`,
    0, 570.1088`, 4.80432`, 6.116957968`, -0.087184`, 0.000817475,
    171.682};
```

Lattice Constant Variation with Temperature
GaSb

T must be input in Celcius for the code to work so a
conversion from T_{kelvin} to $T_{celcius}$ must be made first. The a1 –
a4 variables are constants to correct the lattice constant "a" as the
temperature changes. Latice constant is given in angstroms.

```
t = {8, 10, 12, 20, 30, 40, 50, 60, 70, 80, 85, 100, 120, 140};
T := t - 273.16;
```

```
a0 = 6.095882;

a1 = 3.4963 10^-5;

a2 = 3.3456 10^-8;

a3 = -4.6309 10^-11;

a4 = 2.6369 10^-14;

a[T_] := a0 + a1 T + a2 T^2 + a3 T^3 + a4 T^4

GaSb = a[T]
```
{6.08996, 6.08997, 6.08998, 6.09003,
  6.09012, 6.09021, 6.09033, 6.09045, 6.09059,
  6.09075, 6.09083, 6.0911, 6.09149, 6.09194}

InAs

The α and InAs0 variables are constants to correct the lattice constant "a" as the temperature changes. T is input in Kelvin. Lattice constant is given in angstroms.

```
α = 4.52 10^-6 (*K^-1*);

InAs0 = 6.0583 (*Ang*);
```

$$InAs[T\_] := \frac{InAs0}{E^{298.15\alpha}} E^{\alpha T}$$

```
InAs = InAs[t]
```
{6.05036, 6.05041, 6.05047, 6.05069,
  6.05096, 6.05124, 6.05151, 6.05178, 6.05206,
  6.05233, 6.05247, 6.05288, 6.05342, 6.05397}

InSb

Lattice constant is given in angstroms. T is input in Kelvin.

$$InSb[T\_] := 6.47937 + (6.481 - 6.4785) \frac{(T - 298.15)}{73}$$

```
InSb = InSb[t]
```
{6.46943, 6.4695, 6.46957, 6.46984,
  6.47019, 6.47053, 6.47087, 6.47121, 6.47156,
  6.4719, 6.47207, 6.47258, 6.47327, 6.47395}

Lattice Constant of the Sample

Linear interpolation will be made from the values calculated above. Lattice constant is given in angstroms.

```
InGaSb[x_] := Table[InSb[[i]] * x + GaSb[[i]] * (1 - x),

  {i, 1, 14}]
```

This is the ternary that makes up the wells.

```
Ternary = InGaSb[.35]
```
{6.22277, 6.22281, 6.22284, 6.22297,
  6.22314, 6.22332, 6.22352, 6.22372, 6.22393,
  6.22415, 6.22426, 6.22462, 6.22511, 6.22564}

This is the quaternary that makes up the absorber.

```
InGaSb = InGaSb[.08]
```
{6.12032, 6.12033, 6.12035, 6.12042,
  6.12052, 6.12064, 6.12077, 6.12091, 6.12107,
  6.12124, 6.12133, 6.12161, 6.12203, 6.1225}

```
InGaAsSb[x_] := Table[InGaSb[[i]] * x + InAs[[i]] * (1 - x),
  {i, 1, 14}]
Quaternary = InGaAsSb[.92]
{6.11472, 6.11474, 6.11476, 6.11484,
 6.11496, 6.11509, 6.11523, 6.11538, 6.11555,
 6.11573, 6.11582, 6.11612, 6.11655, 6.11702}
```

Materials Parameters as a Function of Temperature

```
TInAs = Table[InAs[[i]] / 2 * 7, {i, 1, 14}]
{21.1763, 21.1765, 21.1766, 21.1774,
 21.1784, 21.1793, 21.1803, 21.1812, 21.1822,
 21.1832, 21.1836, 21.1851, 21.187, 21.1889}
TTernary = Table[Ternary[[i]] / 2 * 8, {i, 1, 14}]
{24.8911, 24.8912, 24.8913, 24.8919,
 24.8926, 24.8933, 24.8941, 24.8949, 24.8957,
 24.8966, 24.8971, 24.8985, 24.9005, 24.9026}
```

Bibliography

Alfano, R.R., *Semiconductors Probed by Ultrafast Laser Spectroscopy*, Florida: Academic Press, 1984

Anson, S.A., McCahon, S.W., Jang, D.-J., Flatte, M.E., Boggess, T.F., Chow, D.H., Hasenburg, T.C., Grein, C.H. Appl. Phys. Lett. **68**, 15 (1996).

Battacharia, P. *Semiconductor Optoelectronic Devices*, New Jeresey: Prentice-Hall, 1997

Christie, T.P., "Large Aircraft Infrared Countermeasures (LAIRCOM)-FY01 Activity," Excerpt from an unpublished article. http://www.globalsecurity.org/military/library/budget/fy2001/dot-e/airforce/01laircom.html, 2002

Erwin, S.I., "U.S. Warplanes Vulnerable to Shoulder-Fired Missiles," National Defense Magazine, Excerpt from an unpublished article. http://www.nationaldefensemagazine.org/article.cfm?Id-677, 2002

Ferguson, I.T, *Photoluminescence of molecular beam epitaxial grown $Al_{0.48}In_{0.52}As$* j. Vac. Sci. Technol. B **12**, 3 (1994)

Gorski, S., *Carrier Dynamics In Mid-Infrared Quantum Well Lasers Using Time-Resolved Photoluminescence* , AFIT, 2002

Green, G., *Warfighting In The Information Age Emphasized At AOC Symposium*, Journal of Electronic Defense **12**, 21, Horizon House Publishing Inc., 1999

Hepburn, C., "Britney Spears guide to semiconductor physics," Excerpt from an unpublished article. http://britneyspears.ac/lasers.htm, 2002

Jang, D.-J., Flatte, M.E., Grein, C.H. Phys. Rev. B **19**, 58 (1998).

Kaspi, R., Ongstad, A., *High Power and high brightness from an optically pumped InAs/InGaSb type-II midinfrared laser with low confinement*, App. Phys. Let. **81**, 3 (2002)

Landsberg, P.T. *Recombination in Semiconductors*, New York: Cambridge, 1991

Lyon, S.A. *Spectroscopy of hot carriers in semiconductors*, J. Lum. **35**, 121-154 (1986)

Mahr, H. and M.D. Hirsch. "An Optical Up-Conversion Light Gate with Picosecond Resolution," *Optical Communications* **13**(2):96 (February 1975).

Marciniak, M.A. *Optical Characterizaiton of MBE-Grown InAs$_{1-x}$Sb$_x$ Semiconductres on GaSb Substrate*, Dissertation, Air Force Institute of Technology, (August 1995).

McKay, M. *Time-Resolved Photoluminescence of InAs/GaInSb Quantum Well Lasers*, Thesis, Air Force Institute of Technology, (May 2000).

McKelvey, J.P. *Solid state Physics for Engineering and Material Sciences*. Florida: Krieger Publishing, 1993

"Measurements and Characterization," Excerpt from unpublished article. http://www.nrel.gov/measurements/miniority.htm, 2002

Messina, J.W. *IR Countermeasures for Low Observable Aircraft*, 2002

Minority-Carrier Lifetime Spectroscopy, http://www.nrel.gov/measurements/minority.html, 2002

Optoelectronic Project, "Optoelectronic Materials and Devices," Excerpt from an unpublished article. http://www.svec.uh.edu/optp-desc.html, 2002

"Photoluminescence Spectroscopy," Excerpt from an unpublished article. http://www.nrel.gov/measurements/photo.html, 2002

Pike, J. "Electronic Combat Systems," Excerpt from an unpublished article. http://www.fas.org/man/dod.101/sys/ac/equip/ec.htm, 2002

Rockwell, D.L. "Eye on Electronics," Excerpt from an unpublished article. http://www.aiaa.org/market/index.hfm?mar-62&issuetocid-206, 2002

Shah, J., Solid St. Electron. **21**, 43 (1978)

Shah, J. *Ultrafast Spectroscopy of Semiconductors and Semiconductor Nanostrucutres*. Berlin: Springer, 1996.

Vurgaftman, I, Meyer, J.R., Ram-Mohan, L.R. *Band parameters for II-V compound semiconductors and their alloys* Appl. Phys **89**, 11 (2001)

Yaguchi, H. *Photoluminescence Study on Temperature Dependence of Bandgap Energy of GaAsN Alloys*, phys. Stat. Sol. (b) **228**, No.1, 273-277 (2001)

Yamamoto, T., Kasu, M., Noda, S., Sasaki, A. *Photoluminescent properties and optical absorption of AlAs/GaAs disorded superlattices* J.Appl. Phys. **68**, 10 (1990)

Zeghbroeck, B. V. "Carrier Recombination and Generation," Excerpt from an unpublished article. http://ece-www.colorado.edu/~bart/book/book/chapter2/ch2_8.htm, 2002

Vita

       2nd Lieutenant Edward G. Ferguson was born in Texas. His father was an officer in the United States Army and was stationed in Europe for the next several years. Edward attended high school in Colorado Springs, CO. After high school he attended the Colorado School of Mines on a 4-year ROTC scholarship in physics. His Bachelor of Science is in Engineering Physics. He was commissioned on 4 May 2001 and upon graduation from college and completion of the ROTC program there. AFIT is his first assignment on active duty. From AFIT he will be assigned to AFRL/DE, Kirtland AFB, NM where he will serve as a Laser Effects Physicist.

REPORT DOCUMENTATION PAGE

The public reporting burden for this collection of information is estimated to average 1 hour per response, including the time for reviewing instructions, searching existing data sources, gathering and maintaining the data needed, and completing and reviewing the collection of information. Send comments regarding this burden estimate or any other aspect of the collection of information, including suggestions for reducing this burden to Department of Defense, Washington Headquarters Services, Directorate for Information Operations and Reports (0704-0188), 1215 Jefferson Davis Highway, Suite 1204, Arlington, VA 22202-4302. Respondents should be aware that notwithstanding any other provision of law, no person shall be subject to an penalty for failing to comply with a collection of information if it does not display a currently valid OMB control number.
PLEASE DO NOT RETURN YOUR FORM TO THE ABOVE ADDRESS.

1. REPORT DATE (DD-MM-YYYY) 03-10-2002	2. REPORT TYPE Thesis	3. DATES COVERED (From – To) Jan 2003 – March 2003

4. TITLE AND SUBTITLE	5a. CONTRACT NUMBER
Optical Characterization of Antimony-Based, Types-I and -II, Multiple Quantum-Well Semiconductor Structures for Mid-Infrared Laser Applications	5b. GRANT NUMBER
	5c. PROGRAM ELEMENT NUMBER
6. AUTHOR(S) Edward G Ferguson, 2nd Lieutenant, USAF	5d. PROJECT NUMBER
	5e. TASK NUMBER
	5f. WORK UNIT NUMBER

7. PERFORMING ORGANIZATION NAME(S) AND ADDRESS(ES) Air Force Institute of Technology Graduate School of Engineering and Management (AFIT/EN) 2950 P Street, Building 640 WPAFB OH 45433-7765	8. PERFORMING ORGANIZATION REPORT NUMBER AFIT/GAP/ENP/03-04

9. SPONSORING/MONITORING AGENCY NAME(S) AND ADDRESS(ES) Air Force Research Laboratory/Directed Energy Lasers (AFRL/DEL) 3550 Aberdeen Avenue S.E. Kirtland AFB, NM 87117-5776	10. SPONSOR/MONITOR'S ACRONYM(S) AFRL/DEL
	11. SPONSOR/MONITOR'S REPORT NUMBER(S)

12. DISTRIBUTION/AVAILABILITY STATEMENT

APPROVED FOR PUBLIC RELEASE; DISTRIBUTION UNLIMITED.

13. SUPPLEMENTARY NOTES

14. ABSTRACT

This experiment characterizes antimony-based, multiple quantum-well, types-I and -II, semiconductor samples designed for laser applications. The samples emit light in the 3-5-μm range to exploit an atmospheric transmission window, making them ideal for infrared (IR)-seeking missiles countermeasures. Photoluminescence (PL) spectra were collected and yielded bandgap (E_g) dependence-on-temperature relationships. The type-I sample was found to follow the Varshni equation, while the type-II samples showed a rise with temperature in a portion of the curve that should be linear according to the Varshni equation. The type-II samples followed the Varshni equation well at higher temperature. The PL study indicated that the type-I sample had better efficiency than the type-II samples, and that there is some change in efficiency with the waveguide nature of the sample. Carrier temperatures (T_c) were derived from the PL study, all the samples for which T_c was derived operated in the optical phonon regime. The PL data was compared to the "FEMB" computer model and some correlation between the two in recombination energy was seen. A time resolved photoluminescence (TRPL) experiment was conducted using the frequency upconversion technique. The experiment clearly found the upconverted signal, but there was a systematic error that prevented any further analysis of the data.

15. SUBJECT TERMS
photoluminescence, InGaAsSb, InGaSb, FEMB, type-I, type-II, mid-infrared semiconductor lasers

16. SECURITY CLASSIFICATION OF:			17. LIMITATION OF ABSTRACT	18. NUMBER OF PAGES	19a. NAME OF RESPONSIBLE PERSON Lt Col Michael A. Marciniak, ENP
a. REPORT U	b. ABSTRACT U	c. THIS PAGE U	UU	75	19b. TELEPHONE NUMBER (Include area code) (937) 255-3636, ext 4529